

1 **Controls on streamwater age in a saturation overland**
2 **flow-dominated catchment**

3 Dana A. Lapidés^{1,2}, W. Jesse Hahm¹, Daniella M. Rempe³, William E. Dietrich⁴, David
4 N. Dralle²

5 ¹Department of Geography, Simon Fraser University, Burnaby, BC, Canada

6 ²Pacific Southwest Research Station, United States Forest Service, Davis, CA, USA

7 ³University of Texas, Austin, Austin, TX, USA

8 ⁴University of California, Berkeley, Berkeley, CA, USA

9 **Key Points:**

- 10 • Field observations of surface flow, groundwater and saturated extents indicate that satu-
11 ration overland flow dominates streamflow
- 12 • Stable isotope tracers show that stream water age decreases as streamflow increases
- 13 • Streamflow is nevertheless mainly water greater than one day old, meaning that even over-
14 land flow is mostly not event water

Corresponding author: Dana A. Lapidés, dlapides@sfu.ca

Abstract

Water age and flow pathways should be related; however, it is still generally unclear how integrated catchment runoff generation mechanisms result in streamflow age distributions at the outlet. Here, we combine field observations of runoff generation at the Dry Creek catchment with StorAge Selection (SAS) age models to explore the relationship between streamwater age and runoff pathways. Dry Creek is a 3.5 km² catchment in the Northern California Coast Ranges with a Mediterranean climate, and, despite an average rainfall of $\approx 1,800$ mm/yr, is an oak savannah due to the limited water storage capacity. Runoff lag to peak—after initial seasonal wet-up—is rapid (≈ 1 -2 hours), and total annual streamflow consists predominantly of saturation overland flow, based on field mapping of saturated extents and an inferred runoff threshold for the expansion of saturation extent beyond the geomorphic channel. SAS modeling based on daily isotope sampling reveals that streamflow is typically older than one day. Because streamflow is mostly overland flow, this means that a significant portion of overland flow must not be event-rain but instead derive from older, non-event groundwater returning to the surface, consistent with field observations of exfiltrating head gradients, return flow through macropores, and extensive saturation days after storm events. We conclude that even in a landscape with widespread overland flow, runoff pathways may be longer and slower than anticipated. Our findings have implications for the assumptions built into widely used hydrograph separation inferences, namely, the assumption that overland flow consists of new (event) water.

Plain Language Summary

Streams that respond most rapidly to rainfall tend to be fed by a process called overland flow. This study uses high-frequency water tracking measurements to show that even in a watershed fed by overland flow, the water entering the stream during storm events tends to be older than the storm event causing the stream response. Hydrologic measurements made during storm events reveal that water travels through the subsurface before re-emerging as surface flow. The interaction between storm event water and subsurface soils and weathered bedrock likely lead to mixing such that the water entering the stream contains a substantial fraction of water from previous storm events.

1 Introduction

Do distinct runoff pathways give rise to particular streamwater age distributions? Younger streamflow should derive from shorter or faster pathways such as overland flow, whereas older streamflow should derive from longer or slower pathways such as subsurface flow. Streamflow volumes can closely match precipitation input volumes over short timescales (hours-days), but there is widespread evidence—based on early isotopic evidence (e.g., Neal & Rosier, 1990; M. Sklash,

49 1990; Buttle, 1994) and more recent two-component hydrograph separation approaches (e.g., Frey-
50 berg et al., 2018), and fractal (e.g., Kirchner et al., 2000; Godsey et al., 2010) and StorAge Se-
51 lection (SAS) (e.g., Benettin et al., 2017; Visser et al., 2019; Rodriguez & Klaus, 2019) model-
52 ing studies—that stormflow can consist of non-event, older water (sometimes years old) displaced
53 by or driven out of subsurface storage by new water (e.g., Hewlett & Hibbert, 1967). This phe-
54 nomenon indicates that the celerity of a hydraulic perturbation (e.g. a rainfall event) that triggers
55 a runoff response is much faster than the velocity of water in most catchments (e.g., Wilusz et
56 al., 2020; McDonnell & Beven, 2014). Further evidence for the predominance of old water in
57 streamflow comes from the widespread observation that streams are enriched in cations relative
58 to precipitation and commonly exhibit chemostasis (solute concentrations that are relatively in-
59 variant compared to flow) across a range of climates, lithologies, and runoff generation types (Godsey
60 et al., 2009), indicative of the release of water that has resided in the catchment sufficiently long
61 to acquire a characteristic solute concentration. (This timescale may be fairly short in some land-
62 scapes, however, if chemical evolution of waters in the vadose zone occurs rapidly; H. Kim et al.,
63 2017; Anderson et al., 2002).

64 One way to produce young (and dilute) streamwater is for rain to reach the stream by flow-
65 ing over the ground surface as overland flow (Elsenbeer et al., 1994; Elsenbeer & Lack, 1996;
66 Shanley et al., 2002). Relatively abrupt declines of major cation concentrations have been ob-
67 served at a saturation-overland flow (SOF) prone catchment (Dry Creek) at runoff rates of around
68 10 mm/day (W. J. Hahm et al., 2017). Nevertheless, even above these high flow rates when SOF
69 dominated streamflow, perfect dilution of streamwater with rainwater was not observed. This ob-
70 servation suggests either rapid cation exchange reactions that increased the solute concentration
71 of incoming rain as it flowed over the surface (e.g., H. Kim et al., 2017), or significant contribu-
72 tion of relatively high-solute concentration older water to streamflow. These alternative mech-
73 anisms are closely related to whether the source of the streamflow generated from SOF is event
74 rain water or pre-event stored water.

75 SOF occurs when the water table rises from below and intersects the ground surface; the
76 overland component of flow derives both from exfiltrating groundwater (return flow) and direct
77 precipitation on saturated areas (DPSA) (Dunne & Black, 1970a, 1970b; Eshleman et al., 1993).
78 Because the water table is dynamic, the area contributing to SOF can vary over time, which has
79 been referred to as the ‘variable source area’ concept (Dunne & Black, 1970b; Wilson & Diet-
80 rich, 1987). SOF commonly occurs within convergent zones above channel heads (Dunne & Black,
81 1970b; Dunne, 1978; Kidron, 2021) and at the riparian-hillslope interface due to a rapid conver-
82 sion of the tension saturated zone to atmospheric pressure with a small amount of added mois-
83 ture from infiltration (Abdul & Gillham, 1984). SOF has also been documented to occur where
84 small-scale heterogeneities in bedrock properties result in local exfiltrating head gradients (Wilson

85 & Dietrich, 1987). In essence, SOF routes flow over the land surface when the subsurface flow
86 capacity is overwhelmed; this interpretation is commonly reflected in hydrological models, where
87 all water in excess of a shallow subsurface flow capacity threshold is routed to surface flow (e.g.,
88 Beven & Kirkby, 1979; Litwin et al., 2020). Thus, the age of SOF water should reflect the dom-
89 inant source of that runoff, either from the subsurface via return flow (consisting of a mixture of
90 relatively old, pre-event water and event water that has infiltrated) or direct precipitation on sat-
91 urated areas (DPSA, consisting exclusively of newly arriving event water) that never infiltrates.

92 The relationship between hillslope runoff generation and the integrated age distribution at
93 the catchment outlet is still largely opaque because few studies have evaluated travel time distri-
94 bution models in places where runoff generation mechanisms have been directly documented (Wilusz
95 et al., 2020; Rodriguez et al., 2018; Benettin et al., 2017; Putnam et al., 2018). Resolving the im-
96 pact of runoff generation mechanisms on age distributions would help to address the issue of equi-
97 finality in transit time distribution modeling and aid in the interpretation of the controls on stream
98 geochemistry (Li et al., 2020; Torres & Baronas, 2021). Recently, Wilusz et al. (2020) used par-
99 ticle tracking to assess the relationship between runoff generation and transit times, while Rodriguez
100 et al. (2018) compared modeled transit times using a conceptual model of catchment hydrology
101 to empirically calculated transit times with good agreement. Benettin et al. (2017) found that lit-
102 tle streamflow throughout the year was younger than 10 days at the Bruntland Burns site in Scot-
103 land, where saturation overland flow occurs on relatively flat peat-covered areas. Putnam et al.
104 (2018) found that quickflow—which was primarily generated by SOF—was older than event wa-
105 ter (i.e., water that derives from the driving rainfall) at the Pond Branch Catchment in Maryland.
106 M. G. Sklash and Farvolden (1979) found that specific conductance and isotopic composition of
107 overland flow water at the Hillman Creek watershed in Ontario, Canada, implied a strong con-
108 tribution from groundwater. These findings suggest that SOF can be made up primarily of return
109 flow, but controls on the relative fraction of pre-event and event water in SOF remain poorly un-
110 derstood.

111 Water transit time distributions (TTDs) describe the distribution of water ages in fluxes ex-
112 iting a catchment control volume (e.g., Haggerty et al., 2002; Rodhe et al., 1996; Małoszewski
113 & Zuber, 1982). Recently, StorAge Selection (SAS) functions have emerged as a tool for estimat-
114 ing TTDs directly from tracer data with minimal prior assumptions (Botter et al., 2011; Van Der Velde
115 et al., 2012; Harman, 2015). SAS functions define what fraction of outflows (e.g., evapotranspi-
116 ration and streamflow) derive from different water ages in storage. The SAS function framework
117 is grounded in a catchment mass balance; the integrated collection of water ages in storage gives
118 rise to an observed tracer timeseries in effluxes via preferential ‘selection’ of different storage ages.
119 Studies have found that SAS functions vary through time as a function of catchment state (e.g.,
120 Benettin et al., 2017; Harman, 2015; M. Kim et al., 2016), and that streamflow SAS functions

121 tend to show a preference for younger storage water at wetter states, termed the inverse storage
 122 effect (ISE) (e.g., Harman, 2015; Benettin et al., 2017).

123 Here, we combine field observations at the intensively monitored Dry Creek catchment in
 124 Northern California with water age modeling using SAS functions to evaluate how SOF mech-
 125 anisms impact water ages in streamflow. We interpret catchment-integrated isotopic signals in
 126 streamflow with intensive field observations of water storage dynamics, runoff generation, sat-
 127 urated extent, groundwater levels, and head gradients. Specifically, we address the following ques-
 128 tions:

- 129 1. How old is streamflow in a saturation overland flow-dominated catchment?
- 130 2. How does the portion of event water in streamflow change as the dominant runoff gener-
 131 ation mechanism shifts through storm events?
- 132 3. Using transit time models and field observations of runoff generation, what portion of sat-
 133 uration overland flow comes from return flow vs. direct precipitation on saturated areas
 134 (DPSA)?

135 We found that 75% of streamflow is younger than 32 days on average with only 25% of stream-
 136 flow younger than 3 days, and that at high flow states, $\approx 10\%$ of flow derives from the 10% youngest
 137 water in storage (on average < 16 hours old). Field observations reveal the presence of return
 138 flow on the landscape. Comparison between the calculated fraction of SOF in streamflow from
 139 field observations and modeled fraction of streamflow younger than 1 day from SAS modeling
 140 revealed that the majority of overland flow must be older than 1 day. By estimating direct pre-
 141 cipitation on saturated areas (DPSA), we found that even most DPSA must subsequently follow
 142 a subsurface pathway. These findings indicate that SOF is predominantly composed of return flow
 143 and allows us to set a lower bound on the fraction of pre-event water in SOF.

144 2 Methods

145 2.1 Study Site

146 The study catchment, Dry Creek (3.5 km^2 ; outlet at 39.5754° , -123.4642°) is in the Eel River
 147 watershed, in the Northern California Coast Ranges (Figure 1a)) about 200 km north of San Fran-
 148 cisco, in the traditional territory of the Coast Yuki, the California Dene (Athabaskan), and Pomo
 149 (Johnson, 1979; Stewart, 1943; Foster, 1944; Baumhoff & Merriam, 1958). Dry Creek is within
 150 a ranch named Sagehorn, which has been part of the Eel River Critical Zone Observatory since
 151 2015. The site experiences a Mediterranean climate, with a mean annual temperature of 13.3°C
 152 and mean annual precipitation of 1,800 mm (Group, 2013), almost all of which falls as rain be-
 153 tween October-May.

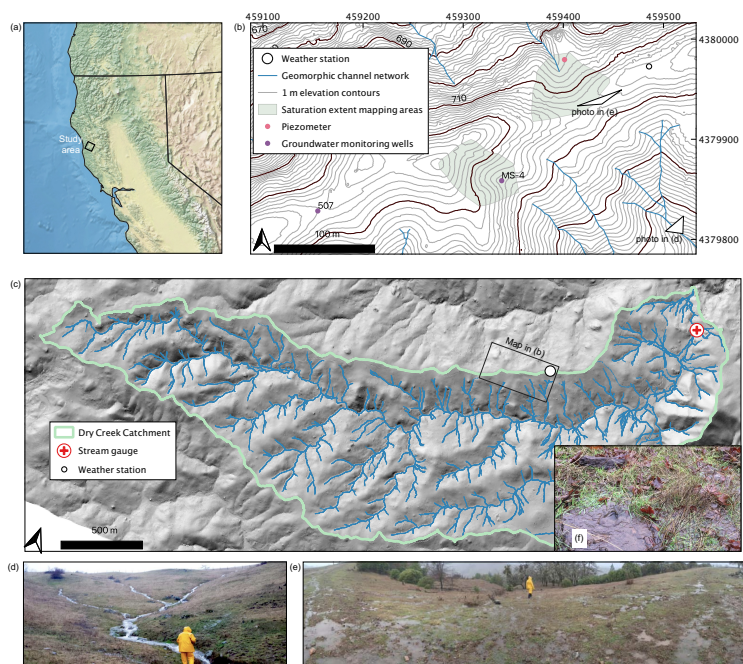


Figure 1. a) Location map of study site in the Northern California Coast Ranges, on Natural Earth hillshade layer. b) Map showing study ridge, with lidar-derived 1-m (thin lines) and 10-m (bold lines) elevation contours. c) Map showing Dry Creek catchment, on lidar-derived hillshade. Blue lines mark the streamflow network calculated from the 1-m DEM. d) Photo of flowing gully network during storm event. e) Panoramic photo of saturated study ridge during storm event. f) Visible return flow through a macropore.

154 The site is underlain by the Central belt *mélange* of the Franciscan complex (Jayko et al.,
 155 1989). The *mélange* bedrock is a sheared argillaceous matrix with embedded blocks of diverse
 156 lithologies, including greywacke (sandstone) and chert. Larger blocks of greywacke cover less
 157 than 15% of the site by surface exposure (Lovill et al., 2018). The primary mineralogy of the *mélange*
 158 matrix is quartz, microcline, albite, muscovite, chlorite, illite, titanite, minor gypsum, pumpel-
 159 lyite and lawsonite, and rare kaolinite and carbonate (Cloos, 1983; W. J. Hahm et al., 2019).

160 Soils developed on the *mélange* matrix are mollisols (Rittiman Jr & Thorson, 2001; W. J. Hahm
 161 et al., 2019). More than 50 pits and augered holes indicate that the soils are typically 50 cm thick
 162 (ranging from 30-70 cm), with an upper organic-rich O horizon and a lower clay-rich Bt hori-
 163 zon. Guelph permeameter measurements of saturated hydraulic conductivity document high con-
 164 ductivities in the near surface that are similar to the maximum recorded rainfall intensities (Dralle
 165 et al., 2018). Pervasive animal burrowing and plant rooting has resulted in abundant macroporos-
 166 ity in the upper portion of the soil.

167 Deep drilling across the site (locations denoted with groundwater monitoring wells mapped
168 in Figure 1b, all well locations shown in W. J. Hahm et al., 2019) revealed that the *in situ* mélange
169 beneath the soils is seasonally unsaturated and weathered to depths of 2 - 4 m (W. J. Hahm et al.,
170 2019), with abundant yellow-red oxidation. Below this depth, the parent material is permanently
171 saturated, blue-black in hue, and has extremely low hydraulic conductivity.

172 Dry Creek drains to the east through a hilly landscape (mean gradient of 28%) typical of
173 the Central belt mélange. A dense gully network is incised into inactive, deep-seated earthflows
174 that have given the site a ‘melted ice-cream’ appearance (Kelsey, 1978). Grazing by sheep (his-
175 torically) and cattle (modern) has been relatively light, and no terracettes have formed. The ge-
176 omorphic channel drainage network (defined by channels with banks and clear elevation contour
177 indentations visible on bare-earth lidar-derived maps) is shown in Figure 1c, and has a relatively
178 high density of 16.9 km/km², with an average upslope contributing area of 1,085 m² at channel
179 heads (Lovill et al., 2018). Hillslopes are convex-up, with typical divide-to-channel horizontal
180 distances of 10 - 20 m (Figure 1). Dry Creek’s catchment-averaged denudation rate, inferred from
181 cosmogenic nuclides in quartz stream sediment, is 0.12 mm/yr (W. J. Hahm et al., 2019). The
182 region has been uplifting and eroding for the past 3 Ma, with the emergence of the Northern Cal-
183 ifornia Coast Ranges from sea-level accompanying the northward migration of the Mendocino
184 Triple Junction (Lock et al., 2006; Atwater & Stock, 1998).

185 The plant community developed on the mélange matrix is an oak savanna (W. Hahm et al.,
186 2017; W. J. Hahm et al., 2018), with primarily European annual herbaceous groundcover that senesces
187 in the summer dry season and a patchy, sparse overstory of winter-deciduous Oregon White Oak
188 (*Quercus garryana*).

189 **2.2 Description of Hydrologic Field Monitoring Infrastructure**

190 The National Center for Airborne Laser Mapping (NCALM) flew lidar at the site in 2015;
191 a 1 m-pixel sized elevation DEM was used to generate the maps in Figure 1. A weather station
192 on the ridgetop records precipitation with a Campbell Scientific TB4 tipping bucket gauge, and
193 is corrected for wind-induced undercatch, as described in (W. J. Hahm et al., 2019). Stream stage
194 is recorded at the outlet with a Solinst Levelogger pressure transducer, with local atmospheric
195 correction. Stream gauging methods are described in (W. J. Hahm et al., 2019).

196 This study capitalizes on the substantial existing monitoring network at Dry Creek to ex-
197 plore SOF (W. J. Hahm et al., 2019, 2020). Nine groundwater monitoring wells were completed
198 with continuously slotted PVC-wells and outfitted with Solinst Levelogger and Campbell Sci-
199 entific CS451 pressure transducers to continuously monitor water table fluctuations; two years
200 of groundwater levels for all wells are shown in (W. J. Hahm et al., 2019), and in this study data

201 from two representative wells are used (MS4 and 507). We installed a 2.54 cm solid PVC piezome-
 202 ter (MNP3) via hand auger to a depth of 55 cm in a side-slope about 5 m horizontally above a
 203 channel head. The lowest 5 cm was slotted and screened, back-filled with sand and sealed with
 204 bentonite. A Solinst pressure transducer was used to monitor head, with 20 cm of casing stick-
 205 up above the ground surface to capture possible artesian conditions. Drilling observations revealed
 206 that the piezometer opening was below the Bt horizon (which was encountered at 35 cm depth),
 207 and within typical smeary, grey-yellow, clay-rich *mélange* matrix weathered bedrock.

208 **2.3 Precipitation and Streamwater Stable Isotopic Composition**

209 **2.3.1 Collection**

210 We measured the stable isotopic composition of hydrogen in both precipitation and stream
 211 water as a tracer for interpreting travel times. The isotope sampling program and analysis meth-
 212 ods were first described in (W. J. Hahm et al., 2020) in a study of oak water sourcing dynamics.
 213 Starting December 10, 2015 through the end of the 2020 water year, precipitation samples were
 214 collected daily when sufficient precipitation had fallen, typically between 06:00-08:00, approx-
 215 imately 1.3 km west of the weather station in an open field at an elevation of 645 m.a.s.l, and stored
 216 in 30 mL HDPE bottles until analysis. When snow fell (which was rare), it was allowed to melt
 217 into the sample collector before sampling. Streamwater samples were collected from near the mouth
 218 of Dry Creek when water was present in the channel on a semi-periodic campaign basis that be-
 219 gan in Fall 2015, followed by two complete years of daily sampling (typically between 8:00-9:00)
 220 during the 2018 and 2019 water years (sampling location = 39°34'22.57"N, 123°27'46.76"W;
 221 3.5 km² drainage area). Groundwater samples were collected on a semi-periodic basis via bailer
 222 from two monitoring wells (MS4 and 507), from a depth ranging from the water table surface
 223 to 1 m below the water table surface.

224 **2.3.2 Analysis**

225 Following the same methodology as described in detail in (W. J. Hahm et al., 2020), all
 226 samples were analyzed at the UC Berkeley Center for Stable Isotope Biogeochemistry via Iso-
 227 tope Ratio Mass Spectroscopy on a Thermo Delta PLUS XL instrument. Data are expressed in
 228 per mil delta notation (‰) relative to Vienna Standard Mean Ocean Water (VSMOW): $\delta D \text{ ‰} =$
 229 $\left(\frac{R_{\text{sample}}}{R_{\text{standard}}} - 1 \right) 1000$, where R is the ratio between the heavy and light isotope (i.e., D to H). The
 230 long-term precision is 0.60‰ δD (W. J. Hahm et al., 2020).

231 To ensure the completeness of the rainfall isotope timeseries, we compared rainfall time-
 232 series from the ridge-top weather station (Figure 1) with the set of timestamps on which precip-
 233 itation was sampled. We identified all time intervals during the study period for which more than
 234 5 mm of rain fell but no sample collection was recorded in the following 48 hours. These crite-

ria were chosen so that rain events reasonably small enough to evaporate and/or transpire completely would not be detected and so that a rain event sampled the next day would not be recorded as missing. We identified 25 dates with missing data (compared to the existing record of 348 samples). Six of the missing samples were likely misplaced prior to sample analysis, and the remaining nineteen were not sampled. When samples were not collected, any rainfall would mix with samples in the following days until the next sample was collected; thus, the next sample collected would represent the average concentration in rainfall over the intervening rainfall events. We replaced missing dates for which no sample was taken with the next measured isotope value if the next sample was taken within 3 days (1 date).

To fill the remaining missing dates, we performed a linear regression between rainfall isotope concentrations at Sagehorn and the nearby Angelo Coast Range Reserve ('Angelo', 23 km northeast; sampling program is described in Oshun et al., 2016)). For all dates with missing Sagehorn rainfall isotope samples, we identified an Angelo rainfall sample as close in time to the missing sample as possible (no more than 2 days later) and used the linear relationship between Sagehorn and Angelo rainfall isotope data to fill in an appropriate value for the missing Sagehorn data. Only ten dates remained with missing data after this process, representing a negligible fraction of precipitation input during the study period.

2.4 Event Runoff Analysis

2.4.1 Lag to Peak

We quantified the lag from rainfall centroid to peak streamflow response for all storm events with well-defined beginnings and ends for both Dry Creek and for the topographically and geologically similar Hank Creek that neighbors Dry Creek to the north (see Lovill et al. (2018) for a map). Hank Creek has a 56% larger catchment area at the gauging location (see maps in Lovill et al., 2018)). The streamflow sensor sampling frequency is 15 minutes, which represents the precision of the analysis.

2.4.2 Runoff Ratio

Graphical hydrograph separation following the method of Hewlett and Hibbert (1967) was performed for 47 Dry Creek storm events spanning the 2016-2019 water years, to quantify how the amount of 'quickflow' generated (the streamflow generated in excess of pre-event 'baseflow') varies in relation to pre-event catchment storage state (quantified by the streamflow magnitude at the start of the event) and storm event size. Events were chosen in such a way that the hydrograph recession was not interrupted by a new rainfall event. As Latron et al. (2008) note, this hydrograph separation approach is arbitrary, and the water volumes separated are not interpreted in terms of runoff pathway origin or age via this method. Although more sophisticated hydro-

269 graph separation methods are available (e.g., Blume et al., 2007), the graphical approach is sim-
 270 ple, has seen widespread and sustained use, and is presented here as a diagnostic that informs catch-
 271 ment rainfall response, similar to the lag-to-peak analysis. Here we also report the event runoff
 272 ratio (quickflow as a fraction of event precipitation).

273 2.5 Surface Saturation—Observations and Model

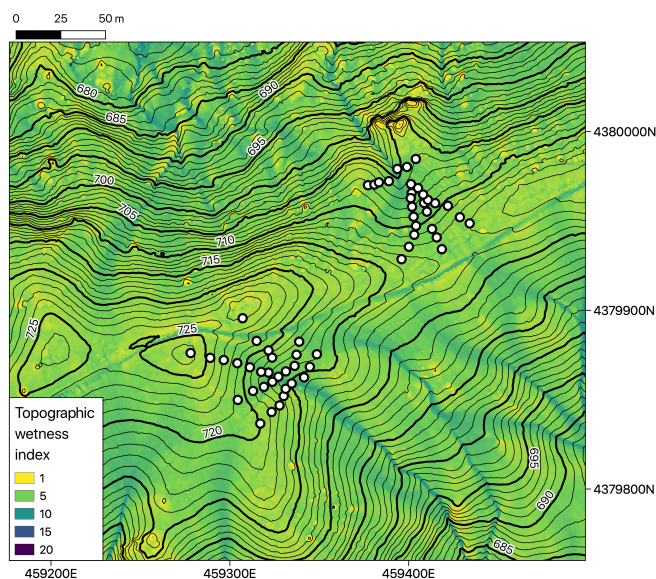


Figure 2. 1-m contour map of the ridge where surface saturation observations were performed. Back-ground colors indicate topographic wetness index, and white circles mark the locations of saturation pits. See Equation 1 for the definition of topographic wetness index.

274 Over the course of a multi-day storm event in January 2018, surface saturation extents were
 275 mapped in two zero-order catchments straddling the northern ridge of Dry Creek (Figure 1). A
 276 total of 57 shallow saturation observation pits (see Figure 2) were dug to a depth of approximately
 277 two centimeters below the soil surface, and marked with flags to facilitate locating. At seven dif-
 278 ferent times corresponding to a range of different flow values in the stream, the pits were logged
 279 as either saturated or not saturated, depending on whether or not a free water surface was observed
 280 in the pits, similar to the qualitative wetness classification presented in Rinderer et al. (2012). It
 281 was assumed that the presence of a free water surface indicated that the shallow water table at
 282 the site had intersected the ground surface at that point, thus potentially contributing to satura-
 283 tion overland flow.

A multi-variate logistic regression was then formulated using the observed saturation data to predict saturation state at all points within the catchment as a function of log-transformed discharge at the catchment outlet, and a topographic wetness index (TWI), calculated as:

$$TWI = \ln \left(\frac{a}{\tan \beta} \right) \quad (1)$$

where a [m] is contributing area per unit length contour (calculated using the r.flow module within GRASS GIS) and β was the topographic slope (Beven & Kirkby, 1979). Calculations were made at a 1 m length scale. Across the observation pits, TWI ranges from 3.1 to 8.8, with a median of 5.0. Across the landscape, the 10th, 50th, and 90th percentile of TWI values are 3.1, 4.6, and 6.4, respectively.

Using the logistic regression model for saturation, the stream discharge record, and a catchment-wide map of TWI, spatially explicit saturation extent maps were generated at all times throughout the period of flow record. At the catchment scale, saturation extent is reported as the percentage of points within the catchment classified as saturated at a given point in time. Note that at the catchment scale, saturated area is effectively a function of discharge in the stream since the spatial distribution of TWI in the catchment is constant. We quantify direct precipitation on saturated areas by multiplying instantaneous rainfall intensities by saturated areas determined from instantaneous streamflow.

2.6 StorAge Selection (SAS) Functions

SAS functions describe quantitatively how waters of different ages are selected from an age-ranked storage distribution to constitute a catchment efflux (ET or streamflow) (Botter et al., 2011; Van Der Velde et al., 2012; Harman, 2015). The basic mass balance is given as:

$$\frac{\delta S_T(T, t)}{\delta t} + \frac{\delta S_T(T, t)}{\delta T} = J(t) - Q(t)\Omega_Q(S_T(T, t), t) - ET(t)\Omega_{ET}(S_T(T, t), t), \quad (2)$$

where t is time [T] and T is age [T]; $S_T(T, t)$ [L] is the system age-rank storage; $J(t)$ [L/T] is precipitation input, $Q(t)$ [L/T] is streamflow output, and $ET(t)$ [L/T] is evapotranspiration output; Ω_Q [-] and Ω_{ET} [-] are SAS functions for Q and ET respectively that determine the output age cumulative distribution function given the age-rank storage at each time. The corresponding SAS functions ω_Q and ω_{ET} are the derivatives with respect to T of Ω_Q and Ω_{ET} . A boundary condition of $S_T(T = 0, t) = 0$ is assumed, and an initial storage $S_T(T, t = 0)$ must be parameterized. Since initial age-rank storage is never known, a spin-up period is used to identify a reasonable catchment state to use as the initial condition.

A conservative tracer can be used to constrain water age distributions in streamflow and evapotranspiration through the following relation:

$$C_Q(t) = \int_0^\infty C_S(T, t) \overleftarrow{p}_Q(T, t) dt, \quad (3)$$

$$C_{ET}(t) = \int_0^{\infty} C_S(T, t) \overleftarrow{p}_{ET}(T, t) dt, \quad (4)$$

where C_Q [\cdot] and C_{ET} [\cdot] are the concentrations of tracer in streamflow and ET respectively, C_S [\cdot] is the distribution of tracer concentration in age-ranked storage, \overleftarrow{p}_Q and \overleftarrow{p}_{ET} are the backward transit time distributions in an output given by:

$$\overleftarrow{p}_Q(T, t) = \frac{\delta\Omega_Q(S_T, t)}{\delta S_T} \frac{\delta S_T}{\delta T}, \quad (5)$$

$$\overleftarrow{p}_{ET}(T, t) = \frac{\delta\Omega_{ET}(S_T, t)}{\delta S_T} \frac{\delta S_T}{\delta T}. \quad (6)$$

Streamflow, precipitation, and concentration inputs are derived from the field monitoring campaign. ET is estimated using the Hargreaves equation. The representation of evapotranspiration (ET) used to parameterize the SAS model likely does not fully capture the dynamics of ET in the Dry Creek catchment since storage trends upwards linearly over time. To correct for this, we adjusted ET based on a running mass balance:

$$S = P - ET - Q \quad (7)$$

306 where S [L/T] is dynamic catchment storage. Over long time periods, catchment storage should
 307 remain approximately constant, but due to errors in flux measurements, particularly ET , S grows
 308 quickly over time. To resolve this, we fit a linear trend to the storage at the end of each dry sea-
 309 son and subtracted this trend from ET to ensure that S remains constant over long timeframes.

We followed the method described by Benettin and Bertuzzo (2018) to calculate the SAS function. Benettin and Bertuzzo (2018) provided a MATLAB implementation of the method, which we translated into the Python programming language (<https://www.python.org/>). An alternate Python implementation was developed by Harman et al. (2019). For a full description of the numerical methods used in this study, see Benettin and Bertuzzo (2018). The only difference is that in our implementation, we use a standard forward Euler numerical scheme, as opposed to the modified Euler method outlined by Benettin and Bertuzzo (2018). Although six options are available in our code, in this study we use a constant power law SAS function for ET:

$$\Omega_{ET} = \left(\frac{S_T(T, t)}{S(t)} \right)^{k_{ET}}, \quad (8)$$

where $S(t)$ is total storage and $k_{ET} \in (0, \infty)$ is a parameter. For the streamflow SAS function, we use a time-varying power law (Benettin et al., 2017):

$$\Omega_Q = \left(\frac{S_T(T, t)}{S(t)} \right)^{k_Q}, \quad (9)$$

where the parameter k_Q [\cdot] varies between a minimum value k_{min_Q} and a maximum value k_{max_Q} with a log-dependence on wetness state w_i :

$$k_Q = k_{min_Q} + (k_{max_Q} - k_{min_Q}) \log[(1 - \logfactor_Q) w_i] \quad (10)$$

310 where w_i is the log-transformed instantaneous stream runoff normalized to the maximum log-
 311 transformed stream runoff at the outlet, and logfactor_Q [·] is a constant parameter. A time-varying
 312 power law has been shown to capture system dynamics well (Benettin et al., 2017), and a log de-
 313 pendence rather than a linear dependence provides more flexibility in how the catchment tran-
 314 sitions from a wet to a dry state due to the addition of an extra parameter. We used the time pe-
 315 riod of October 1, 2017 to October 1, 2018 as a representative spin-up period repeated 10 times
 316 to generate an initial condition for age-rank storage. Model calibration was performed using all
 317 data through the 2019 water year, with the top 95th percentile of parameter sets retained. Model
 318 evaluation was performed on the 2020 water year to evaluate performance of these parameter sets.

Table 1. Parameters tuned in StorAge Selection model using Monte Carlo simulation.

Parameter	Definition
$kmin_Q$	Minimum exponent for Q SAS function as defined in Equation 10 [·]
$kmax_Q$	Maximum exponent for Q SAS function as defined in Equation 10 [·]
logfactor_Q	Scaling between $kmin_Q$ and $kmax_Q$ as defined in Equation 10
k_{ET}	ET SAS function power in Equation 8 [·]
S_0	Initial storage [mm]
C_{S_0}	Initial isotopic concentration in storage [$\delta D\text{‰}$]

We determined best-fit parameter sets by randomly sampling the parameter space (see Ta-
 ble 1 for a list of tuned parameters) via Monte Carlo simulation on 10,000 parameter sets. Pa-
 rameter calibration was done using the set of collected data from October 1, 2016 through Oc-
 tober 1, 2019. We evaluated model fit using the Nash-Sutcliffe model efficiency coefficient (NSE):

$$NSE = 1 - \frac{\sum_{t=1}^{t=t_0} (C_m^t - C_0^t)^2}{\sum_{t=1}^{t=t_0} (C_0^t - \bar{C}_0)^2}, \quad (11)$$

where time t ranges from the beginning ($t = 1$) to the end ($t = t_0$) of the model simulation,
 C_m^t is the modeled streamflow concentration at each time, C_0^t is the observed streamflow concen-
 tration at each time, and \bar{C}_0 is the mean of observed streamflow concentrations (Nash & Sutcliffe,
 1970) and Kling-Gupta Efficiency (KGE):

$$KGE = 1 - \sqrt{(r - 1)^2 + (\alpha - 1)^2 + (\beta - 1)^2}, \quad (12)$$

319 where r is the linear correlation coefficient between modeled and observed data, $\alpha = \sigma_m/\sigma_o$
 320 is the ratio between modeled and observed standard deviation, and $\beta = (\bar{C}_m - \bar{C}_o)/\sigma_o$. $NSE >$
 321 0 or $KGE > -0.41$ indicates that the model performs better than a model defined as the mean of
 322 the data for all time (Knoben et al., 2019). After parameterization, performance was evaluated

323 on data from October 1, 2019 to October 1, 2020. Previous SAS modeling studies which found
324 model performance to be adequate have found maximum NSE ranging from 0.24 to 0.92 (Rodriguez
325 et al., 2021; Rodriguez & Klaus, 2019; Harman, 2015; Benettin et al., 2017; Smith et al., 2018;
326 Van Der Velde et al., 2012), and Kirchner (2003) suggested that a successful behavioral model
327 has $NSE > 0.5$ and $KGE > 0.3$. We rank model performance by the product of NSE and KGE, with
328 successful behavioral performance above 0.15. Using the top 95th percentile of parameter sets,
329 we calculated ensemble means with 25th-75th percentile and 10th-90th percentile uncertainty
330 ranges for: modeled isotope concentration, median storage and streamflow ages, fraction of stream-
331 flow younger than 1 day old, and fraction of streamflow that derives from the youngest 10th per-
332 centile of storage.

333 With a sampling interval of one day, it may be difficult to make robust claims about wa-
334 ter ages at or below the daily timescale. Rodriguez and Klaus (2019) found that a composite SAS
335 function was required to represent isotope dynamics on shorter timescales, a finding that suggests
336 that a higher sampling rate could reveal inadequacies in the functional form of the SAS function
337 used in this study that do not appear in our study as designed. Using a synthetic timeseries of stream
338 isotope data with a high fraction of water younger than 1 day, we explored the impact of coars-
339 ening sampling frequency (unit, 2x, 4x, 8x, 16x) on model calibration results (Supplemental In-
340 formation S4). We found that decreasing the sampling frequency from 1 to 2 or 4 days (coars-
341 ening by 2x or 4x) had a negligible impact on the estimated fraction of water younger than 1 day
342 (unit frequency), indicating that the fraction of water younger than a unit frequency is fairly ro-
343 bust to coarsening in sampling frequency. Thus, a sampling interval of 1 day should be adequate
344 to have confidence in fraction of water younger than 1 day (or even 12h or 6h).

345 **3 Results**

346 **3.1 Catchment Hydrologic Response to Winter Storms**

347 *3.1.1 Hydrograph Features and Runoff Sources*

348 At the end of the summer dry season, shallow and deep unsaturated soil moisture stores
349 and weathered rock moisture are depleted at Dry Creek (W. J. Hahm et al., 2020). The first rains
350 increase moisture content in the unsaturated zone without causing a groundwater response (Dralle
351 et al., 2018). Groundwater responds after approximately 100 mm of cumulative rainfall, and about
352 200 mm is sufficient to raise water tables to or near the ground surface (Dralle et al., 2018). Stor-
353 age then depletes at the start of the dry season, and, as its name implies, Dry Creek typically ceases
354 to flow by late May or early June (Dralle et al., 2018; Lovill et al., 2018).

355 During storm events (example in Figure 3a), large volumes of water commonly exfiltrate
356 via macropore flow (see Figure 4a), and artesian conditions and vertical head gradients are ob-

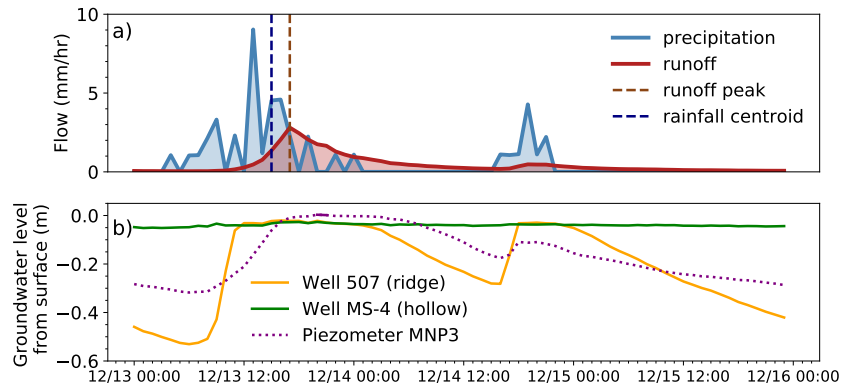


Figure 3. Hydrologic response at Dry Creek in response to a representative wet-season storms on December 12-15, 2018 with a runoff coefficient of 0.54 for the first event. (a) Streamflow is sampled at 15 minute intervals and precipitation is sampled at 5 minute intervals. Both are smoothed to hourly resolution. Lag to peak is 2 hours for the first event. (b) Concurrent groundwater response measured at two wells and one piezometer. Solid line in piezometer data indicates artesian head condition.

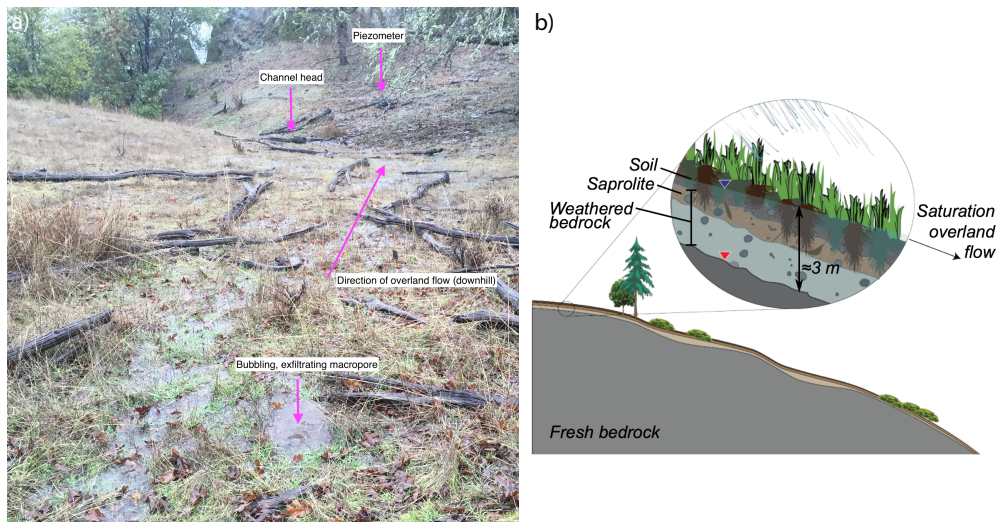


Figure 4. (a) Photo illustrating widespread saturation overland flow, an exfiltrating macropore, and the location of the piezometer on a hillslope above a channel head during a break in the rain on Jan. 17, 2016, 13:20, when the runoff in Dry Creek was 125 mm/day. (b) Conceptual cross-section of the critical zone in the Dry Creek watershed, showing relatively thin weathered zone (≈ 3 m), location of extreme end-member summer (red) and winter (blue) water table locations via inverted triangles, and runoff generation mechanisms. Modified from W. J. Hahm et al. (2019).

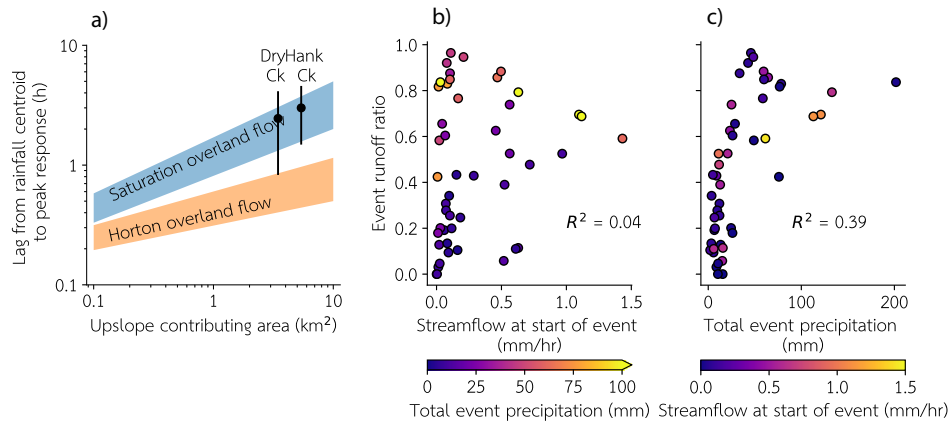


Figure 5. (a) Peak streamflow lag times from rain event centroids (mean \pm 1 s.d.) as a function of drainage area, plotted on regions typical of two overland flow generation mechanisms. Shaded areas and plotting space from Dingman (2015), after Kirkby (1988), based on data from Dunne (1978). (b-c) Event-based runoff ratios at Dry Creek as a function of pre-event streamflow (b) and total event rainfall (c).

357 served in piezometers (solid line in piezometer data in Figures 3b). Periods of time with artesian
 358 head conditions represent a lower bound estimate of the times during which exfiltrating head gra-
 359 dients exist in the catchment. Winter runoff in Dry Creek is dominantly sourced from saturation
 360 overland flow (in the sense of Dunne & Black, 1970b; Dunne, 1978) and shallow subsurface flow
 361 in the weathered portion (upper few meters) of the subsurface, as illustrated schematically in Fig-
 362 ure 4b (Dralle et al., 2018). The subsurface critical zone at Dry Creek consists of a 2 - 4 m thick
 363 layer of organic soils and clay-rich weathered bedrock matrix overlying unweathered, perenni-
 364 ally saturated mélangé, as shown in Figure 4a (W. J. Hahm et al., 2019). The shallow depth to
 365 fresh bedrock results in relatively small integrated porosity and water storage capacity, causing
 366 widespread saturation overland flow during the winter wet season.

367 Lag to peak and event runoff coefficients also support widespread SOF. Across analyzed
 368 storms, Dry Creek's lag to peak time was on average 2.5 ± 1.6 h (± 1 s.d.), and neighboring Hank
 369 Creek's was 3.0 ± 1.5 h, as shown in Figure 5a. These times are typical for catchments of com-
 370 parable area experiencing saturation overland flow according to the commonly depicted timescales
 371 in Dingman (2015)'s *Physical Hydrology* textbook (after Kirkby (1988), based on data from Dunne
 372 (1978)). The event-based runoff ratio at Dry Creek is variable and spans the full range from 0
 373 to 1 (Figure 5b-c). The runoff ratio is uncorrelated with the catchment storage state (wetness) at
 374 the start of a storm event, quantified via the streamflow just before the initial stream response (Fig-
 375 ure 5b). In contrast, the total precipitation in the event explained 39% of the variance in runoff

ratio, with events smaller than 25 mm generally producing runoff ratios less than 0.5, and events greater than 25 mm producing runoff ratios greater than 0.5 (Figure 5c).

3.1.2 Surface Saturation in Response to Storms

Saturation extent measured via discrete mapping campaigns correlated with discharge at the catchment outlet (Figure 6); as discharge decreased in both zero-order catchments (a-f and g-l), the number of saturated pits at both catchments decreased as well. These mapping campaigns spanned nearly the full range of discharge throughout the study period (Figure 7a), and the observation locations' TWI range closely matches that of the catchment at large. The logistic regression model shown in Figure 7a used to predict saturation as a function of catchment discharge and topographic wetness index (TWI) has an accuracy of 83% on observed data.

By applying the logistic regression model, we found that the dynamic extent of saturated area grows throughout a storm event and shrinks as the water table recedes from the surface (Figure 7b; Supplementary Video 1), with portions of the surface of the catchment remaining saturated and contributing to overland flow for days following a precipitation event. At runoff rates with the highest relative runoff contribution, the logistic regression model suggests that more than half of the catchment is saturated (Figure 7a). An instantaneous runoff rate of 2 mm/day at the catchment outlet (not shown) was the threshold above which saturation extends beyond the stream channel, according to the logistic regression model. At runoffs of 10 mm/day, saturation is widespread outside of the channel (Figure 7b). Based on these results, as well as field observations of overland flow corresponding to comparable catchment discharge states, we chose 5 mm/day (best estimate; likely range between 2-10 mm/day) as a threshold runoff rate that corresponds with the maximum subsurface flow capacity adjacent to the channel network, such that the streamflow rate above 5 mm/day derives mostly from saturation overland flow.

3.2 Isotope Dynamics

Isotopic composition of 267 precipitation samples, 460 streamflow samples, and 46 groundwater samples is shown for the full range of flow percentiles in Figure 8d. Streamflow isotopic compositions are markedly damped compared to precipitation, as demonstrated by the larger spread of precipitation isotopes (blue) than streamflow isotopes (red) in the timeseries and dual isotope plots of Figure 8. The sensitivity of streamwater isotopes to precipitation inputs over shorter timescale is shown in Figure 8. Individual samples of streamwater isotopic composition tend to follow a highly damped pattern shifting with the long-term mean, with some larger excursions in the direction of individual rainfall inputs. In general, the relationship between precipitation and streamflow isotopic composition can be highly variable on a storm-to-storm basis. In the zoomed-in view in panel b, streamflow isotopic composition can change little with a large rainfall input (first and

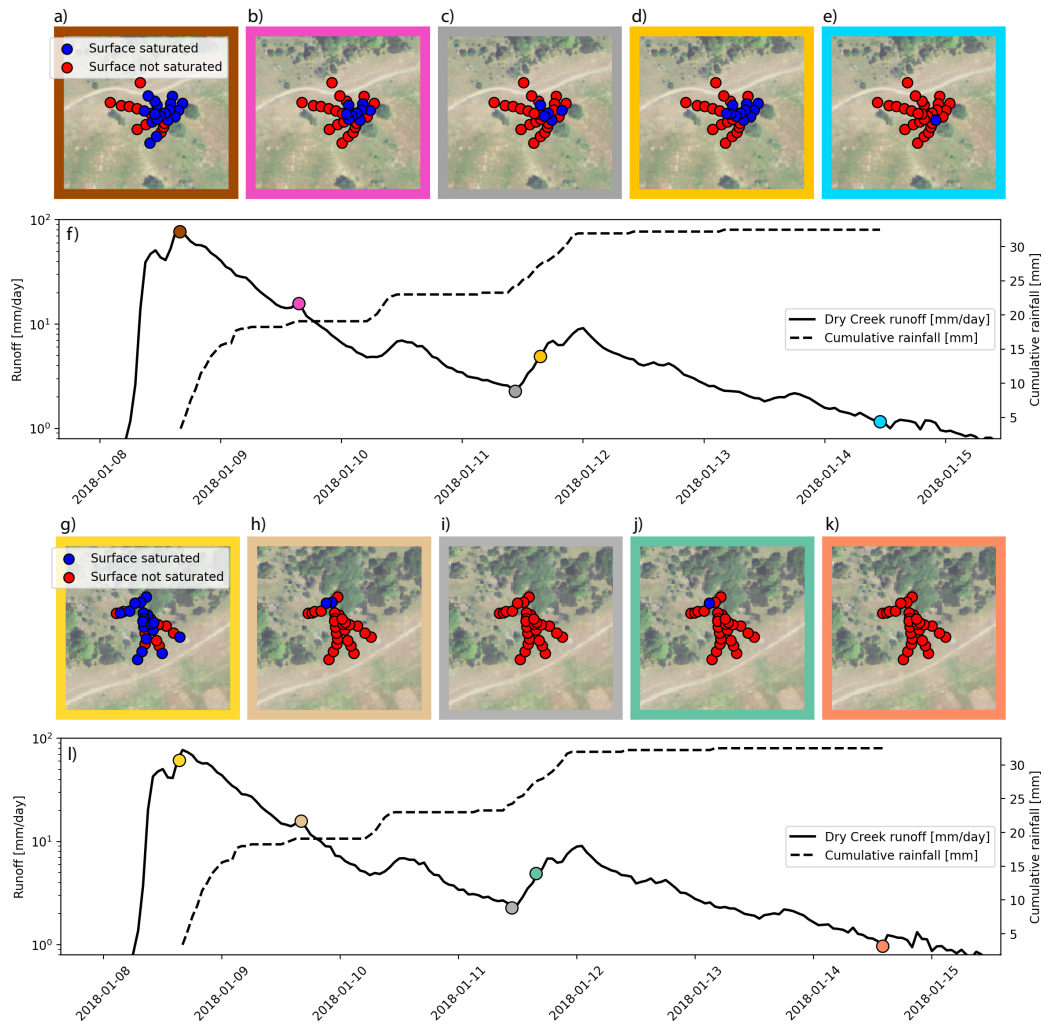


Figure 6. Observations of surface saturation during a streamflow recession in January 2018 at two zero-order catchments (top) in Dry Creek and (bottom) in Hank Creek, bordering Dry Creek. For a map contextualizing the location of the saturation pits, see Figure 2. Panels a-e and g-k show mapped saturation extent during each field visit. Border colors for each panel correspond to the dots with the same color in panel f (a-e) or l (g-k).

410 last large precipitation events) or be displaced significantly (as in the case of the large negative
 411 event) or even the very small negative events in February and March. There is no repeated annual
 412 temporal trend in precipitation isotopic composition, unlike the characteristic sinusoidal signature
 413 of many continental climates (e.g., DeWalle et al., 1997; Allen et al., 2018, 2019). Instead,
 414 we observed a large degree of intra-seasonal scatter in isotopic inputs.

415 At low discharge at the end of the wet season, streamflow samples show evidence of evaporative
 416 enrichment, likely due to evaporation of water in the stream channel during occasional

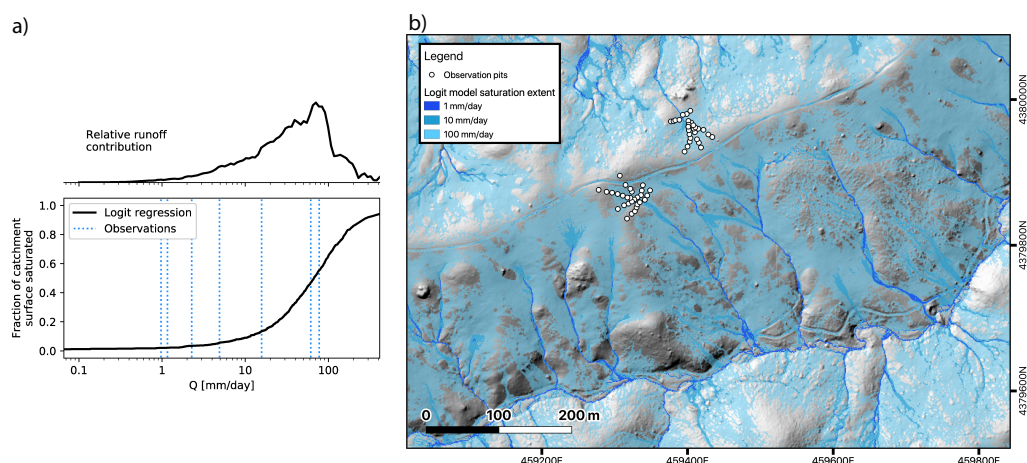


Figure 7. (a) Flow-weighted frequency (top) of instantaneous runoff magnitudes in the Dry Creek catchment. The 5th, 50th, and 95th percentiles flow-weighted frequencies are 20, 90, 320 mm/day, respectively. The median frequency-magnitude flow value coincides with times when a significant (approximately 60% by area) portion of the catchment is saturated, as predicted using the logistic regression model. (b) Saturation extent at different instantaneous streamflow rates. White points show where saturated/not saturated observations were made in field surveys across a range of instantaneous streamflow values. A logistic regression model was fitted using these observations, predicting saturated state at each point in the catchment as a function of log-transformed discharge and topographic wetness index. Blue transparencies over hillshade highlight saturation spatial extent at three discrete streamflow values. Uncolored areas are predicted to not be saturated at an instantaneous streamflow rate of 100 mm/day.

417 long gaps in rain coupled with high atmospheric temperatures. Since evaporative enrichment is
 418 not accounted for in the SAS model, we excluded such samples from the SAS fitting. We iden-
 419 tified a flow threshold of 0.05 mm/day, above which all streamflow isotopic data fell on the me-
 420 teoric water line. At flows below 0.05 mm/day, some streamflow samples were isotopically heavy
 421 and fell on a line with a slope shallower than the local meteoric water line (Supplemental Fig-
 422 ure S8). While not all flows below 0.05 mm/day show an evaporative enrichment signal, this thresh-
 423 old provides a conservative means of excluding evaporative enrichment from calibration.

424 3.3 StorAge Selection Modeling

425 Figure 9 shows SAS modeling results for water year 2019. Results are similar for water year
 426 2020, included in Supplemental Figure S6. Among the top 95th percentile of parameter sets, me-
 427 dian NSE and KGE are 0.62 and 0.82, respectively. The range of NSE and KGE values among
 428 the top 95th percentile are 0.42 - 0.62 (NSE) and 0.82 - 0.83 (KGE). More details on model pa-

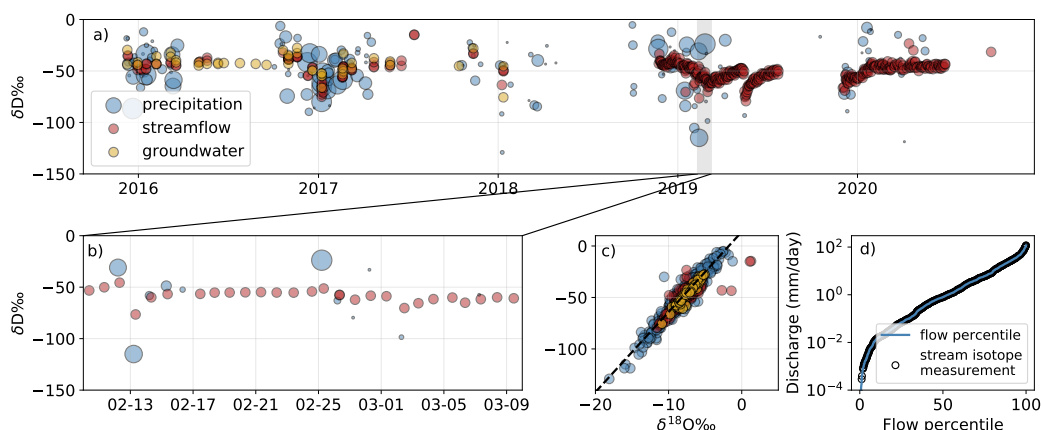


Figure 8. (a) Timeseries of 5 years of daily precipitation sampling, 3 years of episodic and 2 years of daily streamflow sampling, and episodic groundwater sampling with a zoomed-in view for 1 month in (b). In (a) and (b), precipitation isotope markers are scaled by the volume of daily precipitation when the sample was taken. (c) shows dual isotope space for all measurements, and (d) marks the time-weighted flow percentiles at which runoff was sampled.

parameterization can be found in the Supplemental Information S1. As shown in Figure 9b), the SAS model captures the moving average of streamflow isotope data, which shifts in time in response to precipitation inputs (Figure 9a); the model fails to capture the large negative daily excursions January and February and some small positive excursions in December and March. The unexplained large daily excursions suggest that higher temporal resolution in sampling could be beneficial. There is also a period of underestimated streamflow concentration in March-April of 2019, which may be due to a limitation in how the SAS model applies at drier catchment states. While the SAS model has six parameters, results are really only sensitive to two of these parameters (Supplemental Information S1), so additional flexibility in the model structure may be required to capture stream behavior in drier periods. White points, denoting when streamflow is <0.05 mm/day, were excluded from calibration and show an upward trend away from the model, consistent with significant evaporative enrichment (see Supplemental Information S3).

At the end of the dry season, the median ages of water in storage modeled using SAS functions (Figure 9c) are slightly larger than the length of the dry season (5-6 months). At the beginning of the wet season, median streamflow age modeled with SAS functions declines rapidly with high confidence (narrow shaded band) after a short period of rainfall. This timeframe should be related to the time it takes to fill up approximately half of the catchment's dynamic storage capacity (although not identical since streamflow and ET draw preferentially from younger storage). Indeed, the drop in median storage age within the confidence interval occurs at around 150 mm

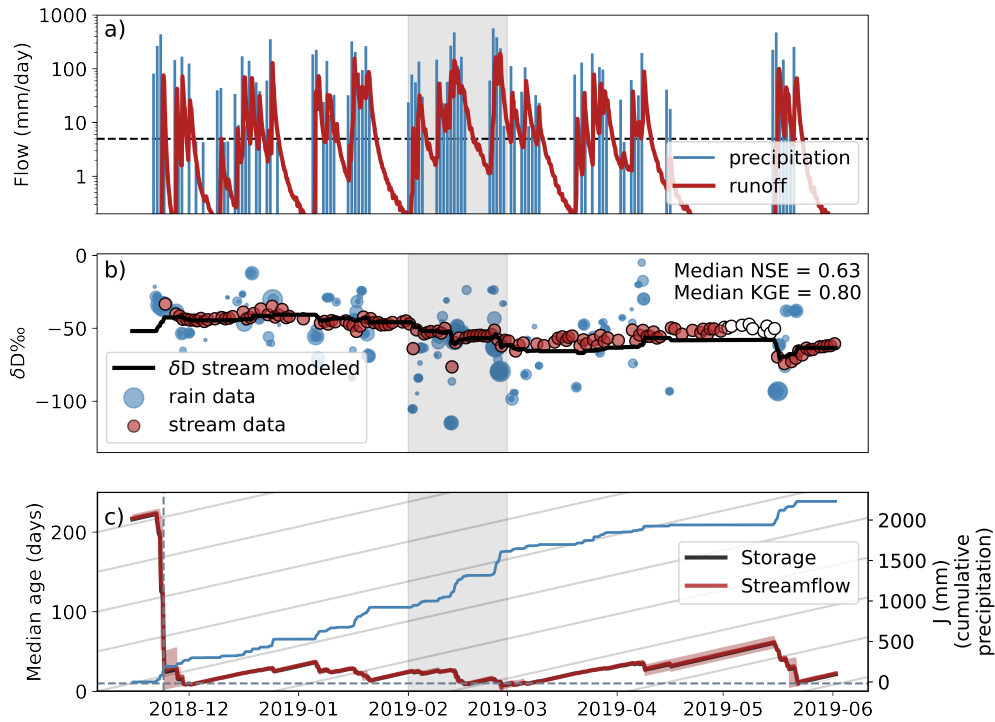


Figure 9. (a) Daily precipitation and instantaneous runoff throughout the wet season 2018-2019. Horizontal dashed black line marks the 5 mm flow threshold above which excess flow is assumed to be SOF. (b) Confidence bars on SAS model predictions (black line) are smaller than the width of the line. The size of plot markers for rainfall data (blue) are scaled by the volume of precipitation. Data shown in white circles are excluded from calibration of the SAS model due to in-channel evaporative enrichment (streamflow <0.05 mm/day). Marked median NSE and KGE are the median values among the top 95th percentile of parameter sets. (c) Shading around median ages indicates 25th-75th percentile of ensemble simulations, and blue line is cumulative precipitation. Storage and streamflow curves lie nearly on top of one another. Vertical dashed line marks cumulative precipitation of 150 mm, and horizontal dashed line marks a median age of 10 days. Shaded vertical bar indicates the timeframe shown in Figure 11.

448 of cumulative precipitation, just a bit more than half of the estimated approximate dynamic stor-
 449 age capacity of the landscape of 200 mm (Dralle et al., 2018; W. J. Hahm et al., 2019; Dralle et
 450 al., 2018). For nearly the whole wet season, median storage age is larger than 10 days (above the
 451 horizontal dashed line in Figure 9c).

452 Median ages of streamflow and storage modeled using SAS functions (Figure 9c) track one
 453 another closely throughout the wet season, falling on top of one another with overlapping con-
 454 fidence intervals. Storage age appears young since the storage modeled by the SAS function is

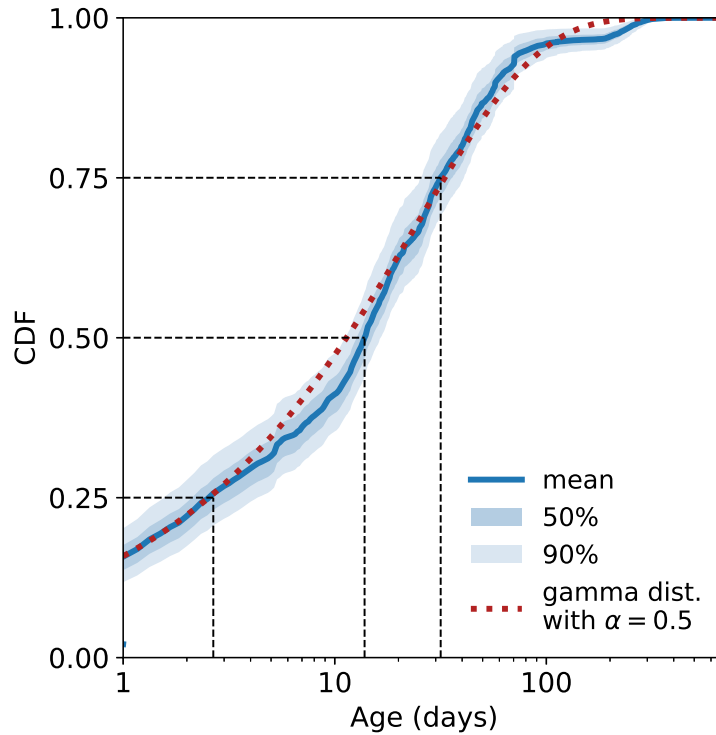


Figure 10. Ensemble mean of flow-weighted average cumulative age distribution function for Dry Creek. Shaded regions show the 25-75th percentiles (50%) and the 5th-95th percentiles (90%) respectively. 25th percentile, median, and 75th percentile of streamflow age are 3 days, 14 days, and 32 days, respectively.

455 only the dynamic portion of storage during the study period. Older storage may exist, but it ac-
 456 counts for only a small portion of dynamic storage so has essentially no impact on median ages.

457 Throughout the study period, the mean age distribution that results from the parameterized
 458 SAS function indicates that essentially all streamflow is younger than 1 year (Figure 10), the ma-
 459 jority of water ($\approx 75\%$) is younger than one month, and about 15% of streamflow is younger than
 460 1 day. More than 90% of streamflow is typically modeled to be younger than 4 months. This find-
 461 ing highlights that the vast majority of streamflow is fairly young, deriving from the current wa-
 462 ter year (i.e., the current wet season), and little long-term storage is included in catchment dis-
 463 charge.

464 **3.4 Overland Flow is Primarily Pre-event Water.**

465 A summary of streamflow contributions from different runoff sources and water of differ-
 466 ent ages estimated via SAS modeling is shown in Table 2 and, for a representative month in 2019,
 467 in Figure 11. Only one month is shown for legibility, but all winter months in the study period

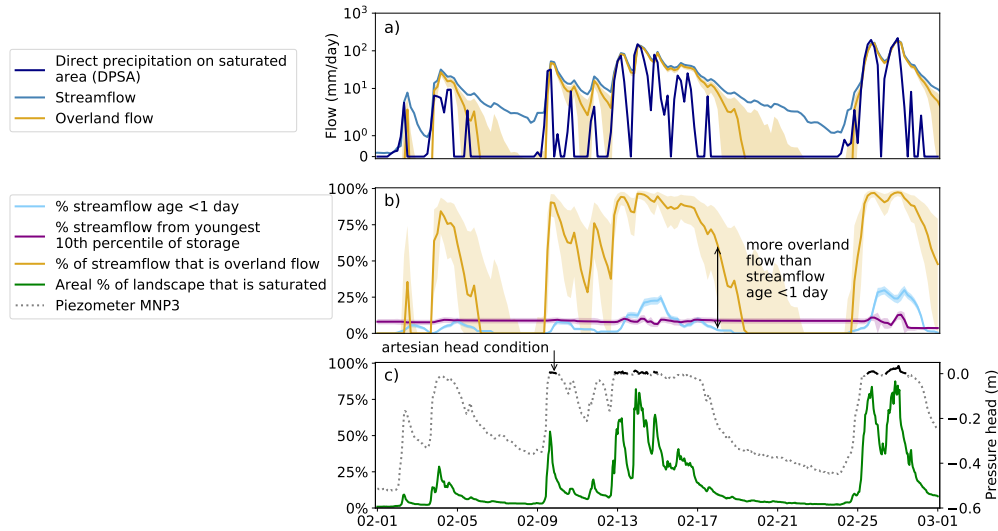


Figure 11. (a) Streamflow, estimated overland flow (streamflow above threshold instantaneous rate), and direct precipitation on saturated area for one representative month in 2019. (b) compares the portion of streamflow derived from overland flow to streamflow water from the youngest 10th percentile of streamflow or water of age <1 day. (c) Piezometer data and areal extents of saturation. Solid portions of piezometer data mark artesian head conditions. Shaded intervals in (a) and (b) denote the 25th-75th percentiles of ensemble simulations except for overland flow. Shaded intervals for overland flow show a range of threshold streamflow values (2-10 mm/day; solid line best estimate of 5 mm/day) for initiation of overland flow throughout the catchment outside of the channel network.

Table 2. Annual streamflow statistics by water year.

Fraction of streamflow that derives from...	WY 2017	WY 2018	WY 2019	WY 2020
overland flow	78%	70%	75%	62%
water age < 1 day	15%	9%	14%	6%
water from youngest 10 th percentile of storage	11%	11%	11%	11%
direct precipitation on saturated area	40%	28%	37%	21%

468 show the same patterns. Using 5 mm/day (likely range of 2-10 mm/day) as the capacity for sub-
 469 surface flow based on the saturation extent mapping analysis (see Figure 7b), we calculated over-
 470 land flow as the difference between instantaneous streamflow and a catchment runoff rate of 5
 471 mm/day (Figure 11a). In this analysis, all of this overland flow is considered to be saturation over-
 472 land flow, as we have not observed any evidence for Horton overland flow at the site. Overland
 473 flow constitutes the majority of streamflow, nearly always accounting for more than 50% of stream-
 474 flow during rainy periods and frequently accounting for more than 90% of flow during large storm

475 events (Figure 11b); in general, overland flow accounts for 62-78% of annual streamflow (Table
476 2). This result is consistent with sustained high groundwater levels during storms (e.g., Figure
477 5b) and the prediction that 80% of the landscape is saturated in large storms (Figure 7a).

478 Figure 11b compares the fraction of streamflow from overland flow to two definitions of
479 new water in streamflow calculated from the 95th percentile of parameter sets for the SAS model:
480 (i) water <1 day old and (ii) water from the youngest 10th percentile of storage. Based on SAS
481 modeling, water from the youngest 10th percentile of storage is consistently about 11% of stream-
482 flow, and only about 10% of streamflow is younger than 1 day on an annual basis (Table 2). Since
483 the SAS model parameterizes the relationship between time series of precipitation isotopes and
484 streamflow isotopes, these model results are driven by the highly damped nature of the stream-
485 flow timeseries compared to the precipitation time series.

486 Only 6-15% of annual streamflow is younger than 1 day, but 62-78% of streamflow derives
487 from overland flow (Table 2). Conservative estimates suggest that surface flow paths from the
488 more distal portion of the watershed would reach the outlet within a day. We can approximate
489 the travel paths as consisting of three distinct elements: sheet runoff on the ≈ 40 m long hillslope
490 (e.g. Figure 1e), focused runoff down hollows and tributary channels (≈ 500 m, e.g., Figure 1d),
491 and travel down the mainstem Dry Creek ($\approx 4,000$ m). Shallow sheet runoff is likely slow (on
492 the order of 0.1 m/min), while in the hollows and channels velocities can exceed 5 m/min, and
493 in the mainstem channel velocities exceed 10 m/min. These very conservative estimates would
494 lead to the more distal part of the overland region reaching the outlet in about 15 hours. Hence,
495 it is likely that overland flow across this landscape, if it remained on the surface and travelled to
496 the outlet, would do so in less than a day.

497 Thus, the finding of significantly more overland flow than water younger than one day indi-
498 cates that a large portion of overland flow must travel through the subsurface to reach the stream.
499 Since all water following a singularly surface flow pathway would reach the outlet in less than
500 1 day, it is possible to set a limit on pre-event water in overland flow by comparing the fraction
501 of streamflow younger than 1 day (light blue line in Figure 11b) to the fraction of streamflow de-
502 rived from overland flow (gold line in Figure 11b). The difference between these two curves gives
503 a lower bound on the pre-event water in overland flow, as marked in Figure 12. In Figure 12, we
504 assumed that (at most) all water age <1 day arrived in the stream by overland flow. Then, given
505 the difference in water volumes, at least 82% of overland flow in must be older than 1 day in wa-
506 ter years 2019-2020. This finding is not unique to these years; throughout the study period, 81
507 - 90% of overland flow must be older than 1 day throughout each water year.

508 Further evidence for the importance of return flow to saturation overland flow comes from
509 estimates of DPSA, calculated as the product of rainfall intensity and the percent saturated area

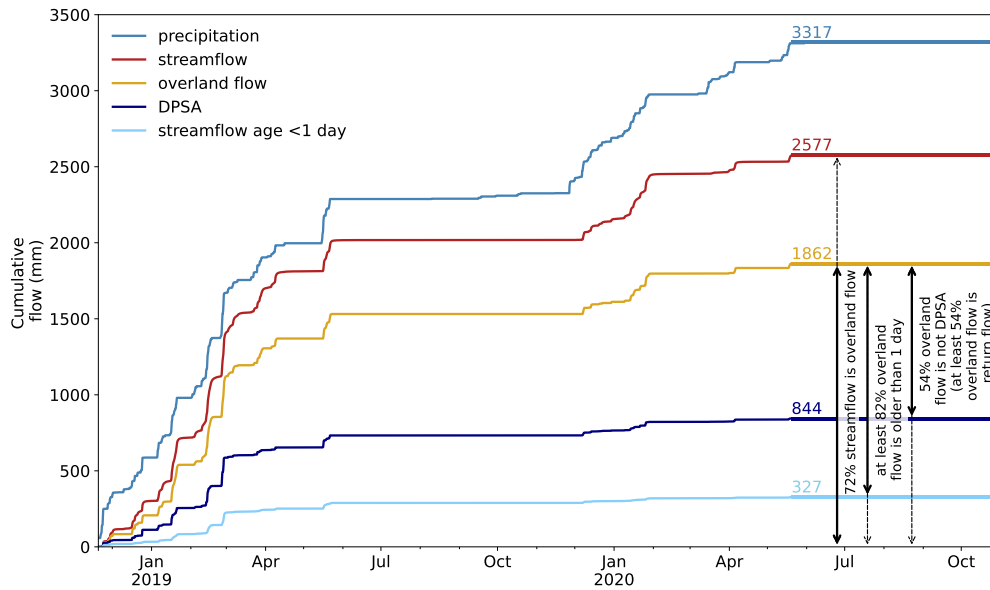


Figure 12. Cumulative amount of precipitation (light blue) compared to streamflow (red), overland flow using a threshold of 5 mm (gold), direct precipitation on saturated area, DPSA, (dark blue), and streamflow age <1 day (light blue). Numbers above each cumulative curve denote cumulative value for WY2019-2020.

510 (Figure 11a). The difference between this DPSA estimate and the overland flow curve places a
 511 different minimum bound on return flow contribution to streamflow since not all rain falling on
 512 saturated area necessarily contributes directly to runoff. Again, we see in Table 2 that at most 21
 513 - 40% of streamflow could have been provided by DPSA, whereas overland flow accounts for 62
 514 - 78% of streamflow on an annual basis. Thus, at least 49 - 66% of overland flow must be gen-
 515 erated via return flow, providing further evidence that return flow plays an important role in sat-
 516 uration overland flow.

517 Overland flow accounts for the vast majority of streamflow, but water younger than 1 day
 518 and DPSA both account for relatively small fractions of annual runoff. These findings indicate
 519 that there must be substantial mixing between surface and subsurface water on the hillslope, which
 520 is also apparent in the damped isotopic signal of streamflow compared to rainfall (Figure 8).

521 4 Discussion

522 4.1 Pre-event Water in Saturation Overland Flow

523 In spite of the thin critical zone and dominance of the saturation overland flow mechanism,
 524 flow that arrives in the stream at Dry Creek is on average days older than the storm that gener-
 525 ated the streamflow. This indicates that: (1) precipitation is stored and overland flow must mix

526 with older, pre-event water; and (2) that water stored between events contributes substantially to
527 saturation overland flow fluxes in events that follow. The storage and mixing have consequences
528 for the conceptualization of runoff generation and water-rock interactions.

529 During periods of low flow (< approximately 2 mm/day), overland flow is not observed,
530 and groundwater levels are below the ground surface across the borehole network. It is not un-
531 til sufficient rains arrive to completely saturate the weathered bedrock and soil zone adjacent to
532 the channel network that water tables intersect the ground surface and saturation overland flow
533 is initiated. Further increases in streamflow are sustained by a continued rise of groundwater ta-
534 bles distal to the channel network and accompanying expansion of saturation extent (Figure 7b),
535 leading to an increasing fraction of runoff that can be attributed to saturation overland flow, i.e.,
536 variable source area (Dunne & Black, 1970b).

537 The apparent paradox of fast streamflow response paired with pre-event water has been ob-
538 served for over 30 years (e.g., Neal & Rosier, 1990; M. Sklash, 1990; Buttle, 1994) and contin-
539 ues to be an active area of hydrologic inquiry (e.g., Kirchner, 2003; Cartwright & Morgenstern,
540 2018). Overland flow, for instance, results in a quick runoff response, and is often considered to
541 represent new (event) water in hydrograph separation literature (e.g., Uhlenbrook et al., 2002;
542 Kronholm & Capel, 2016; Saraiva Okello et al., 2018; Ogunkoya & Jenkins, 1993). Our find-
543 ings directly address the “old-water” paradox by demonstrating that, similar to the shallow sub-
544 surface stormflow observed by Kienzler and Naef (2008), saturation overland flow delivers pre-
545 event water, and thus is older than the age of water delivered by the storm that generates stream-
546 flow. This agrees well with a recent particle tracking study that indicates that overland flow could
547 primarily contain pre-event water while maintaining a streamflow signal that shows a predom-
548 inance of young water catchment-wide (Wilusz et al., 2020). The behavior we observe at Dry Creek
549 is similar to that of the Sleepers River watershed in Vermont, where saturation overland flow was
550 originally documented. There, large extents (up to 50%) of the landscape can be saturated, sat-
551 uration overland flow dominates runoff generation, and yet streamflow is nevertheless still largely
552 older water (Shanley et al., 2015). Similarly, Eshleman et al. (1993), working in the Virginia Coastal
553 Plain, found that saturation overland flow must consist primarily of return flow, based on the pre-
554 dominance of old water in streamflow when saturation overland flow was the primary runoff gen-
555 eration mechanism.

556 Importantly, our results indicate that saturation overland flow and Horton or infiltration ex-
557 cess overland flow should have different signatures in the age distribution of streamflow since in
558 Horton excess overland flow, the interaction with subsurface water pools is likely to be more lim-
559 ited (Horton, 1933, 1945). In the case of Horton overland flow, we would anticipate primarily
560 surface flowpaths and thus delivery of new, event water to streamflow, as has been found in lo-
561 cations where low surface hydraulic conductivity prevents infiltration (e.g., Ribolzi et al., 2007).

4.2 Is There an Inverse Storage Effect in Seasonally Dry Catchments?

The inverse-storage effect (ISE) describes the propensity of catchments to discharge younger water at wetter catchment states (e.g., Harman, 2015; Benettin et al., 2017). This is in contrast to the direct storage effect, where older water makes up the majority of catchment discharge. ISE has been directly observed in laboratory experiments (e.g., M. Kim et al., 2016) and inferred from particle tracking (e.g., Wilusz et al., 2020; Pangle et al., 2017). ISE may be more prevalent in some catchments than others based on particular climates or runoff generation mechanisms. Heidebüchel et al. (2012) found distinct differences in SAS behavior between a semiarid and a humid catchment. Most applications of SAS modeling have been in catchments with limited seasonality, so it is necessary to confirm whether ISE occurs broadly in seasonal catchments; recently, Rodriguez et al. (2018) found that the ISE applies in a catchment with a highly seasonal Mediterranean climate, and in this study we observed a mild ISE effect. Based on parameterization results, the SAS function approximates random sampling behavior as the catchment state becomes drier (less SOF) and exhibits a strong preference for the youngest water in storage at the wettest state (more SOF; see Supplementary Information S1 for details). However, over the course of the study period, the flow-weighted average value of the power exponent k is 0.99 (random sampling is $k = 1$), indicating that most streamflow in Dry Creek is sampled nearly randomly from available storage except during extremely wet periods. Thus, while there is evidence of an ISE at Dry Creek, the overall streamflow signature does not demonstrate a significant inverse storage effect.

While Rodriguez et al. (2018) did find ISE, they found that ISE may not apply at all times in a Mediterranean climate, with a more direct storage effect dominating during transitions between wet and dry seasons in the spring and fall. In our modeling, we allow the SAS function to vary through time according to wetness state, but the relationship between wetness state and SAS function remains constant throughout the study period. As a result, we are unable to determine whether a change in this relationship between wetness state and SAS function behavior occurs at our site. However, Figure 9a (streamflow timeseries in 2019) shows that the runoff goes down to about 0.1 mm/day numerous times over the wet season, indicating significant rapid shifts in catchment wetness throughout the season while the SAS model continues to perform well, missing only a handful of large concentration excursions. Parameterization on 2016-2019 water years also results in similarly good performance on the 2020 water year. There is, however, slightly higher absolute error in modeled concentrations during times of rapid state change versus continuously wet periods (Supplemental Figure S7), and some excursions from the modeled isotopic concentrations correlate with transitions between wet and dry states. This suggests that there may be a direct storage effect during transitions between wet and dry states in the Dry Creek catchment that is not explored in this study. While this effect was not included in our model, these transitions represent a very small portion of the study period so neglecting this effect should have a min-

598 imal impact on the results of this study, particularly since our study focuses on SOF, which oc-
599 curs only once the catchment is wet enough to generate SOF, rather than during transition peri-
600 ods between wet and dry states.

601 **4.3 Assumptions and Limitations**

602 Water age calculations assumed that the entire catchment met a water storage capacity quan-
603 tified as a streamflow threshold; however, the storage capacity of the landscape is met dynam-
604 ically through time so that some parts of the landscape may contribute overland flow before the
605 full storage capacity of the subsurface is met. We do not have data to quantify the extent to which
606 this effect may be important at Dry Creek, although results from a particle tracking study con-
607 ducted by Wilusz et al. (2020) suggest that this effect is minimal. Wilusz et al. (2020) found that
608 maximum groundwater discharge level during different parts of the hydrograph was a function
609 of storage, above which flow derives from overland flow, interflow, or direct runoff (i.e., rain falling
610 directly in the stream channel). Across different portions of the hydrograph, the threshold var-
611 ied by only about a factor of 2. A constant flow threshold, as used in this study, should provide
612 a reasonable estimate for the fraction of streamflow attributable to overland flow over timescales
613 longer than a few hours. Differences in the time to reach storage capacity across the landscape
614 at this temporal resolution should be negligible, and a difference of a factor of 2 is included in
615 the shaded interval in Figure 11b.

616 In our analysis, we have assumed that we can scale our hillslope-scale observations (in lo-
617 cations underlain by *mélange* matrix) to the entire Dry Creek catchment. Lovill et al. (2018), W. J. Hahm
618 et al. (2020), and W. J. Hahm et al. (2019) documented the presence of large sandstone blocks,
619 which cover less than 15% of the catchment by area and behave hydrologically distinctly from
620 the *mélange* matrix areas. In contrast to the *mélange* matrix, the sandstone blocks: i) are deeply
621 weathered; ii) have a thick vadose zone (>5 m), below which fluctuates a seasonal groundwater
622 table; and iii) are observed to be the source of springs that persist into the mid-dry season. Be-
623 cause they are a relatively small portion of the landscape and because we are primarily interested
624 in high-flow dynamics, we opted for the sake of simplicity to not separately model these features.
625 The relatively high model performance (NSE = 0.62) provides some justification for this choice,
626 but future work would benefit from extended analysis of the sandstone blocks, which likely have
627 an outsize contribution to streamflow at low flow states (Lovill et al., 2018).

628 **5 Conclusion**

629 In the Dry Creek catchment in the Northern California Coast Ranges, field observations
630 and stream age modeling using StorAge Selection (SAS) functions reveal that saturation over-
631 land flow arriving in the channel is pre-event water. Field observations reveal that runoff dynam-

632 ics are fast (response within a few hours of rainfall), with runoff coefficients as high as 0.9, and
633 that saturation overland flow is the primary storm runoff mechanism. SAS modeling does not in-
634 dicate much of an inverse storage effect at Dry Creek except at extremely high flows, when younger
635 (as a percentile of storage) streamflow is preferentially discharged. Although streamflow is mod-
636 eled to be relatively young, the SAS model suggests that streamflow is still almost entirely older
637 than 1 day at all times, meaning that streamflow is modeled to be older than event water. Since
638 streamflow is primarily overland flow, the SAS modeling results imply that overland flow must
639 contain a substantial portion of pre-event water. This finding is supported by field observations
640 of exfiltrating head gradients, return flow through macropores, and extensive saturation days af-
641 ter storm events, which collectively point to a significant subsurface origin (i.e., return flow) for
642 the saturation overland flow. Even in this extreme case of full catchment SOF, our analyses in-
643 dicate that substantial mixing of overland flow with subsurface storage must occur to explain the
644 observed streamflow ages.

645 Understanding the relationship between the age of streamflow and runoff generation mech-
646 anisms assists in understanding of how water quality may change over time, particularly under
647 climate change. An increase in extreme precipitation with the same mean, as is expected with
648 climate change in some locations, including California where our site is located (Swain et al., 2018),
649 lead to larger overland flow runoff events. This trend of wet season sharpening is likely to make
650 overland flow more important in catchments where overland flow occurs. Increased precipita-
651 tion volatility is also likely to result in increased relative variability in wetted channel extent (Lapides,
652 Leclerc, et al., 2021), which may apply to saturated area as well. Future studies might consider
653 these interaction and their consequences for kinetic-rate controlled processes like chemical weath-
654 ering.

655 **Open Research**

656 All data and code associated with the manuscript are available at [https://colab.research](https://colab.research.google.com/drive/1fB9BNEY7RzaGpqqnjo7gdeq79Bhqbjvb#scrollTo=znP2tntme3dI)
657 [.google.com/drive/1fB9BNEY7RzaGpqqnjo7gdeq79Bhqbjvb#scrollTo=znP2tntme3dI](https://colab.research.google.com/drive/1fB9BNEY7RzaGpqqnjo7gdeq79Bhqbjvb#scrollTo=znP2tntme3dI)
658 (isotope and groundwater processing code), [https://colab.research.google.com/drive/](https://colab.research.google.com/drive/1EFI1GkU0D1gG56AJ17716U1xXc17W2Yd#scrollTo=1kmoyGsxnuCB)
659 [1EFI1GkU0D1gG56AJ17716U1xXc17W2Yd#scrollTo=1kmoyGsxnuCB](https://colab.research.google.com/drive/1EFI1GkU0D1gG56AJ17716U1xXc17W2Yd#scrollTo=1kmoyGsxnuCB) (SAS modeling code),
660 [https://colab.research.google.com/drive/1VDtkjJGjB0r0mXBq1--CLxVHmDLbGifZ](https://colab.research.google.com/drive/1VDtkjJGjB0r0mXBq1--CLxVHmDLbGifZ?usp=sharing)
661 [?usp=sharing](https://colab.research.google.com/drive/1VDtkjJGjB0r0mXBq1--CLxVHmDLbGifZ?usp=sharing) (logistic regression for saturation extent code), [https://colab.research.google](https://colab.research.google.com/drive/1FzbUSYS60eKA0I02a35qZfktN72Ypzaz)
662 [.com/drive/1FzbUSYS60eKA0I02a35qZfktN72Ypzaz](https://colab.research.google.com/drive/1FzbUSYS60eKA0I02a35qZfktN72Ypzaz) (event runoff coefficient analysis), [https://](https://colab.research.google.com/drive/1F4H-Mb-DfltsCp8mFvXD0ceD7sJVhew5)
663 colab.research.google.com/drive/1F4H-Mb-DfltsCp8mFvXD0ceD7sJVhew5 (lag to peak
664 analysis) and <https://www.hydroshare.org/resource/13244d68f3e74452a8bbc5d8860768c/>
665 (large data files; Lapides, Hahm, et al., 2021).

Acknowledgments

We gratefully acknowledge field access provided by Marilyn and Jerry Russell, and thank Renee Holleman for helping to collect precipitation and stream samples. Wenbo Yang, Todd Dawson, Collin Bode, Hunter Jamison, Sky Lovill, Colleen Murphy, and Sami Cargill contributed to fieldwork and laboratory analyses. Funding was provided by Simon Fraser University, a Natural Science Engineering Research Council of Canada Discovery Grant, the US National Science Foundation-supported Eel River Critical Zone Observatory (EAR 1331940), Oak Ridge Institute for Science and Education (ORISE), the University of California Natural Reserve System Mildred E. Mathias Graduate Student Research Grant, and the Carol Baird Fund for Graduate Field Science.

References

- Abdul, A., & Gillham, R. (1984). Laboratory studies of the effects of the capillary fringe on streamflow generation. *Water Resources Research*, *20*(6), 691–698.
- Allen, S. T., Jasechko, S., Berghuijs, W. R., Welker, J. M., Goldsmith, G. R., & Kirchner, J. W. (2019). Global sinusoidal seasonality in precipitation isotopes. *Hydrology and Earth System Sciences*, *23*(8), 3423–3436.
- Allen, S. T., Kirchner, J. W., & Goldsmith, G. R. (2018). Predicting spatial patterns in precipitation isotope ($\delta^{2}\text{H}$ and $\delta^{18}\text{O}$) seasonality using sinusoidal isoscapes. *Geophysical Research Letters*, *45*(10), 4859–4868.
- Anderson, S., Dietrich, W., & Brimhall, G. (2002). Weathering profiles, mass-balance analysis, and rates of solute loss: Linkages between weathering and erosion in a small, steep catchment. *Geological Society of America Bulletin*, *114*(9), 1143. (00163)
- Atwater, T., & Stock, J. (1998). Pacific-north america plate tectonics of the neogene southwestern united states: an update. *International Geology Review*, *40*(5), 375–402.
- Baumhoff, M. A., & Merriam, C. H. (1958). *California athabaskan groups*. University of California Press.
- Benettin, P., & Bertuzzo, E. (2018). tran-sas v1. 0: a numerical model to compute catchment-scale hydrologic transport using storage selection functions. *Geoscientific Model Development*, *11*(ARTICLE), 1627–1639.
- Benettin, P., Soulsby, C., Birkel, C., Tetzlaff, D., Botter, G., & Rinaldo, A. (2017). Using sas functions and high-resolution isotope data to unravel travel time distributions in headwater catchments. *Water Resources Research*, *53*(3), 1864–1878.
- Beven, K. J., & Kirkby, M. J. (1979). A physically based, variable contributing area model of basin hydrology/un modèle à base physique de zone d'appel variable de l'hydrologie du bassin versant. *Hydrological Sciences Journal*, *24*(1), 43–69.
- Blume, T., Zehe, E., & Bronstert, A. (2007, October). Rainfall—runoff response, event-

- 702 based runoff coefficients and hydrograph separation. *Hydrological Sciences Journal*,
 703 52(5), 843–862. Retrieved 2021-07-16, from [https://doi.org/10.1623/hysj.52](https://doi.org/10.1623/hysj.52.5.843)
 704 [.5.843](https://doi.org/10.1623/hysj.52.5.843) (Publisher: Taylor & Francis _eprint: <https://doi.org/10.1623/hysj.52.5.843>)
 705 doi: 10.1623/hysj.52.5.843
- 706 Botter, G., Bertuzzo, E., & Rinaldo, A. (2011). Catchment residence and travel time distribu-
 707 tions: The master equation. *Geophysical Research Letters*, 38(11).
- 708 Buttle, J. (1994). Isotope hydrograph separations and rapid delivery of pre-event water from
 709 drainage basins. *Progress in physical geography*, 18(1), 16–41.
- 710 Cartwright, I., & Morgenstern, U. (2018). Using tritium and other geochemical tracers to
 711 address the “old water paradox” in headwater catchments. *Journal of Hydrology*, 563,
 712 13–21.
- 713 Cloos, M. (1983). Comparative study of melange matrix and metashales from the francis-
 714 can subduction complex with the basal great valley sequence, california. *The Journal*
 715 *of Geology*, 91(3), 291–306.
- 716 Craig, H. (1961). Isotopic variations in meteoric waters. *Science*, 133(3465), 1702–1703.
- 717 DeWalle, D., Edwards, P., Swistock, B., Aravena, R., & Drimmie, R. (1997). Seasonal
 718 isotope hydrology of three appalachian forest catchments. *Hydrological Processes*,
 719 11(15), 1895–1906.
- 720 Dingman, S. L. (2015). *Physical hydrology*. Waveland press.
- 721 Dralle, D. N., Hahm, W. J., Rempe, D. M., Karst, N. J., Thompson, S. E., & Dietrich, W. E.
 722 (2018). Quantification of the seasonal hillslope water storage that does not drive
 723 streamflow. *Hydrological processes*, 32(13), 1978–1992.
- 724 Dunne, T. (1978). Field studies of hillslope flow processes. *Hillslope hydrology*, 227–293.
- 725 Dunne, T., & Black, R. D. (1970a). An experimental investigation of runoff production in
 726 permeable soils. *Water Resources Research*, 6(2), 478–490.
- 727 Dunne, T., & Black, R. D. (1970b). Partial area contributions to storm runoff in a small new
 728 england watershed. *Water resources research*, 6(5), 1296–1311.
- 729 Elsenbeer, H., & Lack, A. (1996, May). Hydrometric and hydrochemical evidence for fast
 730 flowpaths at La Cuenca, Western Amazonia. *Journal of Hydrology*, 180(1), 237–
 731 250. Retrieved 2019-11-16, from [http://www.sciencedirect.com/science/](http://www.sciencedirect.com/science/article/pii/0022169495028897)
 732 [article/pii/0022169495028897](http://www.sciencedirect.com/science/article/pii/0022169495028897) doi: 10.1016/0022-1694(95)02889-7
- 733 Elsenbeer, H., West, A., & Bonell, M. (1994, October). Hydrologic pathways and stormflow
 734 hydrochemistry at South Creek, northeast Queensland. *Journal of Hydrology*, 162(1),
 735 1–21. Retrieved 2019-11-16, from [http://www.sciencedirect.com/science/](http://www.sciencedirect.com/science/article/pii/002216949400027)
 736 [article/pii/002216949400027](http://www.sciencedirect.com/science/article/pii/002216949400027) doi: 10.1016/0022-1694(94)90002-7
- 737 Eshleman, K. N., Pollard, J. S., & O’Brien, A. K. (1993). Determination of contribut-
 738 ing areas for saturation overland flow from chemical hydrograph separations.

- 739 *Water Resources Research*, 29(10), 3577–3587. Retrieved 2021-07-21, from
 740 <http://agupubs.onlinelibrary.wiley.com/doi/abs/10.1029/93WR01811>
 741 (_eprint: <https://onlinelibrary.wiley.com/doi/pdf/10.1029/93WR01811>) doi:
 742 10.1029/93WR01811
- 743 Foster, G. M. (1944). *A summary of yuki culture* (Vol. 50). University of California Press
 744 Berkeley, CA.
- 745 Freyberg, J. v., Studer, B., Rinderer, M., & Kirchner, J. W. (2018). Studying catchment storm
 746 response using event-and pre-event-water volumes as fractions of precipitation rather
 747 than discharge. *Hydrology and Earth System Sciences*, 22(11), 5847–5865.
- 748 Gallart, F., Valiente, M., Llorens, P., Cayuela, C., Sprenger, M., & Latron, J. (2020). In-
 749 vestigating young water fractions in a small mediterranean mountain catchment: Both
 750 precipitation forcing and sampling frequency matter. *Hydrological Processes*, 34(17),
 751 3618–3634.
- 752 Godsey, S. E., Aas, W., Clair, T. A., De Wit, H. A., Fernandez, I. J., Kahl, J. S., . . . others
 753 (2010). Generality of fractal 1/f scaling in catchment tracer time series, and its im-
 754 plications for catchment travel time distributions. *Hydrological Processes*, 24(12),
 755 1660–1671.
- 756 Godsey, S. E., Kirchner, J. W., & Clow, D. W. (2009). Concentration–discharge relationships
 757 reflect chemostatic characteristics of us catchments. *Hydrological Processes: An Inter-
 758 national Journal*, 23(13), 1844–1864.
- 759 Group, P. C. (2013). *PRISM Climate Data* (Tech. Rep.). Oregon State University. Retrieved
 760 from <http://prism.oregonstate.edu> (00000)
- 761 Haggerty, R., Wondzell, S. M., & Johnson, M. A. (2002). Power-law residence time distribu-
 762 tion in the hyporheic zone of a 2nd-order mountain stream. *Geophysical Research Let-
 763 ters*, 29(13), 18–1.
- 764 Hahm, W., Dralle, D., Lovill, S., Rose, J., Dawson, T., & Dietrich, W. (2017). Exploratory
 765 tree survey (2016- eel river critical zone observatory- sagehorn- central belt melange,
 766 franciscan complex, northern california coast ranges, usa). hydroshare. *HydroShare*.
- 767 Hahm, W. J., Dietrich, W. E., & Dawson, T. E. (2018). Controls on the distribution and
 768 resilience of quercus garryana: ecophysiological evidence of oak’s water-limitation
 769 tolerance. *Ecosphere*, 9(5), e02218.
- 770 Hahm, W. J., Dralle, D. N., Dawson, T. E., & Dietrich, W. E. (2020). Oak transpiration
 771 drawn from the weathered bedrock vadose zone in the summer dry season. *Water Re-
 772 sources Research*.
- 773 Hahm, W. J., Rempe, D. M., Dralle, D. N., Dawson, T. E., Lovill, S. M., Bryk, A. B., . . .
 774 Dietrich, W. E. (2019). Lithologically controlled subsurface critical zone thickness
 775 and water storage capacity determine regional plant community composition. *Water*

- 776 *Resources Research*, 55(4), 3028–3055.
- 777 Hahm, W. J., Wang, J., Druhan, J. L., Rempe, D., & Dietrich, W. E. (2017). Relating runoff
778 generation mechanisms to concentration-discharge relationships in catchments with
779 well-characterized critical zone structures and hydrologic dynamics. *AGUFM*, 2017,
780 B43E–2172.
- 781 Harman, C. J. (2015). Time-variable transit time distributions and transport: Theory and
782 application to storage-dependent transport of chloride in a watershed. *Water Resources*
783 *Research*, 51(1), 1–30.
- 784 Harman, C. J., Evans, O., & Lu, F. (2019). *mesas*. ([https://github.com/charman2/](https://github.com/charman2/mesas)
785 [mesas](https://github.com/charman2/mesas))
- 786 Heimbüchel, I., Troch, P. A., Lyon, S. W., & Weiler, M. (2012). The master transit time dis-
787 tribution of variable flow systems. *Water Resources Research*, 48(6).
- 788 Hewlett, J. D., & Hibbert, A. R. (1967). Factors affecting the response of small watersheds to
789 precipitation in humid areas. *Forest hydrology*, 1, 275–290.
- 790 Horton, R. E. (1933). The role of infiltration in the hydrologic cycle. *Eos, Transactions*
791 *American Geophysical Union*, 14(1), 446–460.
- 792 Horton, R. E. (1945). Erosional development of streams and their drainage basins; hy-
793 drophysical approach to quantitative morphology. *Geological society of America bul-*
794 *letin*, 56(3), 275–370.
- 795 Jayko, A., Blake, M., McLaughlin, R., Ohlin, H., Ellen, S., & Kelsey, H. (1989). *Recon-*
796 *naissance geologic map of the covelo 30-by 60-minute quadrangle, northern california*
797 (Tech. Rep. No. MF-2001). US Government Printing Office.
- 798 Johnson, S. G. (1979). *The land-use history of the coast range preserve, Mendocino County,*
799 *California* (Unpublished doctoral dissertation). San Francisco State University, San
800 Francisco, CA.
- 801 Kelsey, H. M. (1978). Earthflows in franciscan melange, van duzen river basin, california.
802 *Geology*, 6(6), 361–364.
- 803 Kidron, G. J. (2021). Comparing overland flow processes between semiarid and humid
804 regions: does saturation overland flow take place in semiarid regions? *Journal of Hy-*
805 *drology*, 593, 125624.
- 806 Kienzler, P. M., & Naef, F. (2008). Subsurface storm flow formation at different hillslopes
807 and implications for the ‘old water paradox’. *Hydrological Processes: An Interna-*
808 *tional Journal*, 22(1), 104–116.
- 809 Kim, H., Dietrich, W. E., Thurnhoffer, B. M., Bishop, J. K., & Fung, I. Y. (2017). Controls
810 on solute concentration-discharge relationships revealed by simultaneous hydrochem-
811 istry observations of hillslope runoff and stream flow: The importance of critical zone
812 structure. *Water Resources Research*, 53(2), 1424–1443.

- 813 Kim, M., Pangle, L. A., Cardoso, C., Lora, M., Volkmann, T. H., Wang, Y., . . . Troch, P. A.
814 (2016). Transit time distributions and storage selection functions in a sloping soil
815 lysimeter with time-varying flow paths: Direct observation of internal and external
816 transport variability. *Water Resources Research*, 52(9), 7105–7129.
- 817 Kirchner, J. W. (2003). A double paradox in catchment hydrology and geochemistry. *Hydro-*
818 *logical processes*, 17(4), 871–874.
- 819 Kirchner, J. W., Feng, X., & Neal, C. (2000). Fractal stream chemistry and its implications
820 for contaminant transport in catchments. *Nature*, 403(6769), 524–527.
- 821 Kirkby, M. (1988). Hillslope runoff processes and models. *Journal of Hydrology*, 100(1-3),
822 315–339.
- 823 Knoben, W. J., Freer, J. E., & Woods, R. A. (2019). Inherent benchmark or not? compar-
824 ing nash–sutcliffe and kling–gupta efficiency scores. *Hydrology and Earth System Sci-*
825 *ences*, 23(10), 4323–4331.
- 826 Kronholm, S. C., & Capel, P. D. (2016). Estimation of time-variable fast flow path chemi-
827 cal concentrations for application in tracer-based hydrograph separation analyses. *Wa-*
828 *ter Resources Research*, 52(9), 6881–6896.
- 829 Lapidés, D. A., Hahm, W. J., Rempe, D. M., Dietrich, W. E., & Dralle, D. N.
830 (2021). *Calculating streamwater age using storage selection func-*
831 *tions at dry creek, ca.* (HydroShare, [https://www.hydroshare.org/](https://www.hydroshare.org/resource/13244d68f3e74452a8bbcb5d8860768c/)
832 [resource/13244d68f3e74452a8bbcb5d8860768c/](https://www.hydroshare.org/resource/13244d68f3e74452a8bbcb5d8860768c/)) doi: 10.4211/hs
833 .13244d68f3e74452a8bbcb5d8860768c
- 834 Lapidés, D. A., Leclerc, C. D., Moidu, H., Dralle, D. N., & Hahm, W. J. (2021). Variability
835 of stream extents controlled by flow regime and network hydraulic scaling. *Hydrologi-*
836 *cal Processes*. doi: 10.1002/hyp.14079
- 837 Latron, J., Soler, M., Llorens, P., & Gallart, F. (2008). Spatial and temporal variability of
838 the hydrological response in a small Mediterranean research catchment (Vallcebre,
839 Eastern Pyrenees). *Hydrological Processes*, 22(6), 775–787. Retrieved 2021-04-
840 14, from <https://onlinelibrary.wiley.com/doi/abs/10.1002/hyp.6648>
841 (_eprint: <https://onlinelibrary.wiley.com/doi/pdf/10.1002/hyp.6648>) doi: [https://](https://doi.org/10.1002/hyp.6648)
842 doi.org/10.1002/hyp.6648
- 843 Li, L., Sullivan, P. L., Benettin, P., Cirpka, O. A., Bishop, K., Brantley, S. L., . . . others
844 (2020). Toward catchment hydro-biogeochemical theories. *Wiley Interdisciplinary*
845 *Reviews: Water*, e1495.
- 846 Litwin, D. G., Tucker, G. E., Barnhart, K. R., & Harman, C. J. (2020). Groundwaterdupuit-
847 percolator: A landlab component for groundwater flow. *Journal of Open Source Soft-*
848 *ware*, 5(46), 1935.
- 849 Lock, J., Kelsey, H., Furlong, K., & Woolace, A. (2006). Late neogene and quaternary land-

- 850 scape evolution of the northern california coast ranges: Evidence for mendocino triple
851 junction tectonics. *Geological Society of America Bulletin*, 118(9-10), 1232–1246.
- 852 Lovill, S., Hahm, W., & Dietrich, W. (2018). Drainage from the critical zone: Lithologic
853 controls on the persistence and spatial extent of wetted channels during the summer
854 dry season. *Water Resources Research*, 54(8), 5702–5726.
- 855 Małoszewski, P., & Zuber, A. (1982). Determining the turnover time of groundwater systems
856 with the aid of environmental tracers: 1. models and their applicability. *Journal of hydrology*, 57(3-4), 207–231.
- 857 McDonnell, J. J., & Beven, K. (2014). Debates—the future of hydrological sciences: A
858 (common) path forward? a call to action aimed at understanding velocities, celerities
859 and residence time distributions of the headwater hydrograph. *Water Resources Research*, 50(6), 5342–5350.
- 860 Nash, J. E., & Sutcliffe, J. V. (1970). River flow forecasting through conceptual models part
861 i—a discussion of principles. *Journal of hydrology*, 10(3), 282–290.
- 862 Neal, C., & Rosier, P. T. (1990). Chemical studies of chloride and stable oxygen isotopes in
863 two conifer afforested and moorland sites in the british uplands. *Journal of Hydrology*,
864 115(1-4), 269–283.
- 865 Ogunkoya, O., & Jenkins, A. (1993). Analysis of storm hydrograph and flow pathways using
866 a three-component hydrograph separation model. *Journal of Hydrology*, 142(1-4), 71–
867 88.
- 868 Oshun, J., Dietrich, W. E., Dawson, T. E., & Fung, I. (2016). Dynamic, structured heterogeneity
869 of water isotopes inside hillslopes. *Water Resources Research*, 52(1), 164–
870 189.
- 871 Pangle, L. A., Kim, M., Cardoso, C., Lora, M., Meira Neto, A. A., Volkmann, T. H., . . .
872 Harman, C. J. (2017). The mechanistic basis for storage-dependent age distributions
873 of water discharged from an experimental hillslope. *Water Resources Research*, 53(4),
874 2733–2754.
- 875 Putnam, S. M., et al. (2018). *The influence of landscape structure on storage and streamflow
876 generation in a piedmont catchment* (Unpublished doctoral dissertation). Johns Hopkins
877 University, Baltimore, MD.
- 878 Riboldi, O., Karambiri, H., Bariac, T., Benedetti, M., Caquineaux, S., Descloitres, M., &
879 Aventurier, A. (2007). Mechanisms affecting stormflow generation and solute behaviour
880 in a sahelian headwater catchment. *Journal of hydrology*, 337(1-2), 104–116.
- 881 Rinderer, M., Kollegger, A., Fischer, B. M., Stähli, M., & Seibert, J. (2012). Sensing with
882 boots and trousers—qualitative field observations of shallow soil moisture patterns.
883 *Hydrological Processes*, 26(26), 4112–4120.
- 884 Rittiman Jr, C., & Thorson, T. (2001). Soil survey of mendocino county. *California, Western*
885

- 887 *Part, Mendocino County Resource Conservation District.*
- 888 Rodhe, A., Nyberg, L., & Bishop, K. (1996). Transit times for water in a small till catch-
889 ment from a step shift in the oxygen 18 content of the water input. *Water Resources*
890 *Research*, 32(12), 3497–3511.
- 891 Rodriguez, N. B., & Klaus, J. (2019). Catchment travel times from composite storage selec-
892 tion functions representing the superposition of streamflow generation processes. *Wa-*
893 *ter Resources Research*, 55(11), 9292–9314.
- 894 Rodriguez, N. B., McGuire, K. J., & Klaus, J. (2018). Time-varying storage–water age re-
895 lationships in a catchment with a mediterranean climate. *Water Resources Research*,
896 54(6), 3988–4008.
- 897 Rodriguez, N. B., Pfister, L., Zehe, E., & Klaus, J. (2021). A comparison of catchment travel
898 times and storage deduced from deuterium and tritium tracers using storage selection
899 functions. *Hydrology and Earth System Sciences*, 25(1), 401–428.
- 900 Saraiva Okello, A. M. L., Uhlenbrook, S., Jewitt, G. P., Masih, I., Riddell, E. S., & Van der
901 Zaag, P. (2018). Hydrograph separation using tracers and digital filters to quantify
902 runoff components in a semi-arid mesoscale catchment. *Hydrological Processes*,
903 32(10), 1334–1350.
- 904 Shanley, J. B., Kendall, C., Smith, T. E., Wolock, D. M., & McDonnell, J. J. (2002). Con-
905 trols on old and new water contributions to stream flow at some nested catchments
906 in Vermont, USA. *Hydrological Processes*, 16(3), 589–609. Retrieved 2021-07-21,
907 from <http://onlinelibrary.wiley.com/doi/abs/10.1002/hyp.312> (_eprint:
908 <https://onlinelibrary.wiley.com/doi/pdf/10.1002/hyp.312>) doi: 10.1002/hyp.312
- 909 Shanley, J. B., Sebestyen, S. D., McDonnell, J. J., McGlynn, B. L., & Dunne, T. (2015).
910 Water’s Way at Sleepers River watershed – revisiting flow generation in a post-glacial
911 landscape, Vermont USA. *Hydrological Processes*, 29(16), 3447–3459. Retrieved
912 2021-07-21, from <http://onlinelibrary.wiley.com/doi/abs/10.1002/hyp.10377> (_eprint: <https://onlinelibrary.wiley.com/doi/pdf/10.1002/hyp.10377>) doi:
913 10.1002/hyp.10377
- 914
- 915 Sklash, M. (1990). Environmental isotope studies of storm and snowmelt runoff generation.
916 *Process studies in hillslope hydrology*, 401–436.
- 917 Sklash, M. G., & Farvolden, R. N. (1979). The role of groundwater in storm runoff. *Journal*
918 *of Hydrology*, 43(1-4), 45–65.
- 919 Smith, A., Tetzlaff, D., & Soulsby, C. (2018). On the use of storage selection functions to as-
920 sess time-variant travel times in lakes. *Water Resources Research*, 54(7), 5163–5185.
- 921 Stewart, O. C. (1943). *Notes on pomo ethnogeography*. University of California Press.
- 922 Swain, D. L., Langenbrunner, B., Neelin, J. D., & Hall, A. (2018, May). Increasing precip-
923 itation volatility in twenty-first-century California. *Nature Climate Change*, 8(5), 427–

- 924 433. doi: 10.1038/s41558-018-0140-y
925 Torres, M. A., & Baronas, J. J. (2021). Modulation of Riverine Concentration-
926 Discharge Relationships by Changes in the Shape of the Water Transit Time
927 Distribution. *Global Biogeochemical Cycles*, 35(1), e2020GB006694.
928 Retrieved 2021-07-16, from [https://agupubs.onlinelibrary](https://agupubs.onlinelibrary.wiley.com/doi/abs/10.1029/2020GB006694)
929 [.wiley.com/doi/abs/10.1029/2020GB006694](https://agupubs.onlinelibrary.wiley.com/doi/abs/10.1029/2020GB006694) (_eprint:
930 <https://agupubs.onlinelibrary.wiley.com/doi/pdf/10.1029/2020GB006694>) doi:
931 10.1029/2020GB006694
- 932 Uhlenbrook, S., Frey, M., Leibundgut, C., & Maloszewski, P. (2002). Hydrograph separa-
933 tions in a mesoscale mountainous basin at event and seasonal timescales. *Water Re-*
934 *sources Research*, 38(6), 31–1.
- 935 Van Der Velde, Y., Torfs, P., Van Der Zee, S., & Uijlenhoet, R. (2012). Quantifying
936 catchment-scale mixing and its effect on time-varying travel time distributions. *Water*
937 *Resources Research*, 48(6).
- 938 Visser, A., Thaw, M., Deinhart, A., Bibby, R., Safeeq, M., Conklin, M., . . . Van der Velde,
939 Y. (2019). Cosmogenic isotopes unravel the hydrochronology and water storage
940 dynamics of the southern sierra critical zone. *Water Resources Research*, 55(2),
941 1429–1450.
- 942 Wilson, C., & Dietrich, W. (1987). The contribution of bedrock groundwater flow to storm
943 runoff and high pore pressure development in hollows. *IAHS-AISH publication*(165),
944 49–59.
- 945 Wilusz, D., Harman, C., Ball, W., Maxwell, R., & Buda, A. (2020). Using particle track-
946 ing to understand flow paths, age distributions, and the paradoxical origins of the
947 inverse storage effect in an experimental catchment. *Water Resources Research*, 56(4),
948 e2019WR025140.